# *chrna3* modulates alcohol response


## Authors

Joshua Raine[1], Caroline Kibat [1, 2, #], Tirtha Das Banerjee [3], Antónia Monteiro[3], Ajay S. Mathuru [1, 2, 4, 5, 6 *]

## Affiliations

1. Department of Physiology, Yong Loo Lin School of Medicine, National University of Singapore, Singapore, Singapore, 117593
2. Yale-NUS College, National University of Singapore, Singapore, Singapore, 138527
3. Department of Biological Sciences, National University of Singapore, Singapore, Singapore, 117558
4. Institute for Digital Medicine (WisDM), Yong Loo Lin School of Medicine, National University of Singapore, Singapore, 117456
5. Institute of Molecular and Cell Biology, A*STAR, Singapore, Singapore, 138673
6. Healthy Longevity Translational Research Programme, Yong Loo Lin School of Medicine, National University of Singapore, Singapore, Singapore, 117596

*Correspondence: ajay.mathuru@nus.edu.sg # At the time the work was performed


1

## Abstract

Alcohol use disorders (AUDs) are complex phenomena governed by genetics, neurophysiology, environment, and societal structures. New methods to understand the underlying neurogenetics are valuable for designing personalised interventional strategies. Here, we used a two-choice self-administration zebrafish assay (SAZA) to isolate the function of nicotinic acetylcholine receptor (nAChR) subunit alpha3 (*chrna3*) in alcohol response. Juvenile zebrafish, prior to sex differentiation, were examined in this study. They exhibited a biphasic response when self-administering alcohol that transitioned from attraction to aversion within minutes, suggesting they can regulate exposure to alcohol. This inverted U-shaped self-administration mirrored the effect alcohol has on shoaling behaviour. Exposure to low concentration of alcohol reduced anxiety-like behaviours, while sedative effects became prominent at higher concentrations resulting in reduced locomotion and uncoordinated swimming. In contrast, these responses are blunted in *chrna3* mutants. They exhibited prolonged alcohol self-administration, and increased gregariousness. Transcriptomic analyses suggest that glutamatergic and GABAergic neurotransmission alongside cholinergic signalling is impacted in the mutant brains. Our results thus suggest that *chrna3* dysfunction has a systemic change with an increase in alcohol tolerance being one effect. These findings also highlight the use of non-rodent alternatives to understand the neurogenetics of development of AUD.

## Keywords:

Zebrafish, Preclinical model, Alcohol Use Disorders, SUD, Hormesis, *CHRNA3*

## Introduction

Substance use disorders (SUDs), encompassing nicotine, alcohol, and opioid abuse, represent a significant global health burden, accounting for approximately 162.5 million disability-adjusted life years lost worldwide (Rehm and Shield, 2019a; Moeller and Terplan, 2020). According to the WHO, harmful alcohol use alone is estimated to have resulted in 5.3% of deaths across the world in 2022 (Rehm and Shield, 2019b; Witkiewitz et al., 2019; Aslam and Kwo, 2023). Efforts to understand the interplay among social, environmental, and biological factors to effectively counter alcohol use disorders (AUDs) continue to be a focus area, as the response to alcohol in vertebrates itself is a complex multifactorial phenomenon. Alcohol interacts with a range of neuromodulatory systems, engages reward processing circuits, and affects multiple neurotransmitter systems, including glutamate and GABA neurotransmission (Chvilicek et al., 2020). Both genetic and neurobiological factors contribute significantly to AUD development (Egervari et al., 2021; Koob and Vendruscolo, 2023). Thus, a comprehensive understanding of these factors, while accounting for individual variability, is crucial for developing effective AUD prevention and interventional strategies (Witkiewitz et al., 2019; Yang et al., 2022; Aslam and Kwo, 2023).

Animal models are indispensable for dissociating genetic contributors to the development of substance dependence in humans (Smith, 2020). While such studies are typically conducted in mammalian models, high operating costs can hinder studies on genetic variability and small, single gene effects (Cox, 2015; de Magalhães, 2015). Zebrafish present a cost-effective alternative, combining high throughput genetic manipulation with whole-brain live neural activity imaging (Cully, 2019). Additionally, anatomical and functional conservation with mammalian sub-cortical circuitry is now well established (Kily et al., 2008; Gerlai, 2020).

Zebrafish exhibit behavioural and physiological responses to psychoactive substances that are consistent with mammals, providing construct validity, however, studies have primarily employed indirect

47 measures, like place preference or avoidance assays (Echevarria et al., 2011; Tsang et al., 2019). These
48 are useful, but are considered inadequate to model SUD (Smith, 2020). Despite the difficulty in designing
49 contingent, self-administration assays for aquatic animals, they are essential to gain predictive validity
50 (Smith, 2020). Few studies have explored active choice (Schneider et al., 2023) or self-administration
51 (Sterling et al., 2015; Bossé and Peterson, 2017; Nathan et al., 2022). Among these, studies with
52 juveniles (~4-5 weeks), as reported here, offer an advantage over both larvae or adults as behavioural
53 responses become more consistent by this age, and a relatively large number of individuals can be
54 examined to detect small effects.

55 Here, we expanded on the Self-Administration Zebrafish Assay (SAZA) (Nathan et al., 2022) to study
56 *chrna3*'s role in acute, dynamic alcohol responses. Human genetic studies consistently associate single
57 nucleotide polymorphisms (SNPs) in the *CHRNA5-A3-B4* cluster, encoding nicotinic acetylcholine
58 receptor (nAChR) subunits α5, α3, and β4, with nicotine addiction by GWAS (Thorgeirsson et al., 2008;
59 Amos et al., 2010; Bierut, 2011). Rare variants in *CHRNA3* have been linked to alcohol dependence in
60 humans (Haller et al., 2014; Kamens et al., 2023). While investigations into contributions of *CHRNA5* and
61 *CHRNB4* to SUD have progressed rapidly using rodent models (Fowler et al., 2011; Frahm et al., 2011),
62 such models for *CHRNA3* are fewer due to neonatal lethality of knock-outs (Xu et al., 1999; Elayouby et
63 al., 2021). This leaves the role of *CHRNA3* in alcohol dependence unclear and correlational. Our study
64 fills this gap, validating *chrna3*'s contribution to the acute alcohol response.

65 Using SAZA for juvenile zebrafish, we report an acute biphasic response to alcohol, transitioning rapidly
66 from attraction to avoidance. This correlates with the proposed role of alcohol as both stimulant and
67 sedative. *chrna3* mutants showed alcohol tolerance, blunting the avoidance response and resisting
68 changes to shoaling behaviour. In the context of the Genetically Informed Neurobiology of Addiction
69 (Bogdan et al., 2023), our study provides new evidence that variations in *CHRNA3* may directly influence
70 predisposition to alcohol addiction in humans.

71 # Materials & Methods

72 ## Fish husbandry

73 Zebrafish (*D. rerio*, ABWT) were housed, bred, and reared as described by Nathan *et al.*, 2022(Nathan et
74 al., 2022) at the ZebraFish Facility (Institute of Molecular and Cell Biology, A*STAR) in groups of 20–30 in
75 3-L tanks under standard facility conditions. All experimental protocols involving zebrafish were
76 approved by the Institutional Animal Care and Use Committee (IACUC) of the Biological Resource Center
77 at A*STAR. Approved experimental protocols (IACUC #201529, # 231808) were followed.

78 ## Generation of c*hrna3* mutant zebrafish

79 The full details of zebrafish gene editing by CRISPR/Cas9 have been described by Hwang *et al. (Hwang et*
80 *al., 2013)*. CRISPR targets were determined using the web tool 'chop-chop' for the exon 5 region to
81 disrupt key functional domains. Oligonucleotides containing the identified CRISPR target sequence
82 ($GGN_{20}$), along with a universal reverse primer encoding the sgRNA scaffold, were used to generate a
83 transcription template, following the method described by Bassett et al. (Bassett et al., 2013). The
84 sequences of these oligonucleotides are listed in Table 1. CRISPR target sites are underlined, and
85 homology arms are shown in lowercase letters. Zebrafish embryos (nacre background) were injected at
86 the 1-cell stage with 1 nL of a mixture containing 1 µL sgRNA (≈ 4-5 µg) and 1 µL Cas9 mRNA (≈1 µg). Fish
87 were genotyped by fin-clipping and sequencing of genomic DNA at 10 weeks post-injection to identify
88 founder fish (F0). The identified founder fish were outcrossed to AB background WT fish to obtain F1
89 embryos. F1 embryos from each outcrossed family were collected and some of the embryos were
90 verified by sequencing. Once germline transmission was confirmed by sanger sequencing, the remaining
91 embryos were grown to adulthood. Homozygous *chrna3*$^{C246X/C246X}$ mutants (AB x nacre mixed

92 background) from the F3 generation onwards were used for all subsequent experiments, alongside WT
93 equivalents, and are henceforth referred to as *chrna3*$^{C246X}$.
94

95 ## Self-administration for zebrafish assay (SAZA) apparatus setup

96 The SAZA assay apparatus was set up as described in (Nathan et al., 2022), outlined briefly as follows.
97 The assay tank was constructed of opaque, 3mm thick acrylic to be 35 x 75 x 30mm (width × length ×
98 height). One end of the zone contained a dividing sheet of the same material, 30mm in length, to split
99 the zone into two halves while still permitting access (Figure 1A). The zone was placed on an LED
100 lightbox for illumination, providing 5000 lux at maximum intensity (LightPad LX Series, Artograph, USA).
101 Video footage was captured at 30 frames per second using an acA2040-90µM USB3.0 Basler camera.
102 Solutions were dispensed from vertically mounted 10ml syringes through silicon tubing (outer diameter:
103 1/16", inner diameter 1/32") into the corner of their designated zone, mediated via solenoid pinch
104 valves (Automate Scientific, USA, SKU: 02-pp-04i) (Figure 1A). System water was consistently supplied to
105 the tank through additional silicon tubing at the opposite end of the tank to the divided zones and was
106 removed at a matching rate (~2ml per minute) by gravitational siphoning from the end of the dividing
107 sheet near the centre of the tank (Figure 1A). This created a consistent flow and stopped dispensed
108 solutions from escaping their designated zones while permitting access to the fish being assayed
109 (Nathan et al., 2022). CRITTA (http://www.critta.org), a custom LABVIEW software, was used to track
110 fish movements as described by Krishnan *et al.* (2014) (Krishnan et al., 2014). The tracking system was
111 configured so that only the entry of the fish to a designated region of interest would trigger the pinch
112 valve to release and dispense the corresponding solution.

## Alcohol concentration measurement

Alcohol concentrations in the SAZA stimulus zone were measured using a DensitoPro (Mettler-Toledo), returning the measured solution to the zone with minimal disturbance. As attempting to measure the concentration of alcohol during a live fish assay would disturb the fish and prevent a natural response, an artificial dispensing scheme of ten continuous seconds per minute followed immediately by measurement was used as a substitute (Figure 1C). This was based on the average time fish spent in the stimulus zone under assorted alcohol dispensing solutions over 18 minutes of exposure (Table 2). After 12 minutes, the dispensing cycle was halted, but measurements continued to estimate the effect the outflow rate had on concentration in the zone if no stimulus was dispensed for a long period.

The assay was repeated three times per concentration of alcohol (20, 70%).

## SAZA

SAZA was performed as described in (Nathan et al., 2022), outlined briefly as follows. First, 40 ml of system water was added to the tank, the in and outflow tubes were inserted into their respective conditions, and the flow of system water started. One zebrafish of 30-35 dpf was taken directly from its husbandry tank and added gently to each SAZA tank, then given ~5 minutes to adjust and recover post-transfer until consistent swimming behaviour had resumed and the fish had explored all zones of the SAZA tank. The recording and tracking scheme was then started for 24 minutes, consisting of three consecutive periods; three minutes of pre-exposure, 18 minutes of self-administration stimulus delivery, and three minutes post-exposure. Only during the 18-minute stimulus delivery period would entry to a designated zone trigger dispensing of the corresponding solution (Figure 1A). The valve opening time was set to a minimum of five seconds per entry. The stimuli delivered were 0/20/70% absolute alcohol diluted in the facility system water. Following each assay, the zone was emptied of all liquid, washed,

136 and refilled before adding the next fish. The volume of each solution dispensed was also recorded. To
137 reduce bias, the zone designated to deliver the stimulus solution was randomly assigned to be either the
138 left or right and changed periodically throughout the experiment such that ~50% of the fish were tested
139 in each configuration. Around 30 fish naive to SAZA were assayed per concentration of alcohol.
140 Following each assay, the fish were euthanized. Juvenile fish, ~5 weeks old, were used for all
141 behavioural experiments as this developmental stage offers the advantages of more complex locomotor
142 behaviour and reduced individual variability over younger larvae, while possessing comparable
143 structural brain development to adult fish, yet still facilitating higher throughput and practicality of assay
144 design.

145 SAZA Data analysis

146 SAZA data outputs from CRITTA were processed by custom Python scripts. These provided data on time
147 spent in each zone and mean velocity in each zone used in these analyses. The data were separated into
148 three major time groups; pre-exposure, total stimulus delivery period, and post-exposure. The stimulus
149 delivery period was then further subdivided into either start and end (0-9m/9-18m), or three minute
150 segments (0-3m/3-6m/6-9m, etc…) for further analyses.

151 The preference index (PI) was calculated as the ratio of the difference between the times spent in the
152 stimulus and control zones relative to the total time spent in the two zones. The PI for a given duration
153 ($PI_X$) was calculated by the following formula; $PI_X$ = (TinS - TinC) / (TinS + TinC), where TinS = time in
154 stimulus zone (s) and TinC = time in control zone (s). This gives the value for PI maximum bounds of + or
155 - 1 indicating more time spent relatively in the stimulus or control, respectively. For example, a PI of +1
156 would indicate 100% of relative time spent in the stimulus zone during one time period. Delta PI
157 between two time periods ($\Delta PI_{X-Y}$) was calculated as $\Delta PI_{XY} = PI_Y - PI_X$ , where $PI_X$ = the earlier period, and
158 $PI_Y$ = the later period. This gives the value for ΔPI maximum bounds of + or - 2, with the values indicating

159 the direction and magnitude of the change in preference from the first time point to the second. For
160 example, a ΔPI of +2 would indicate a change from 100% relative time spent in the control zone in the
161 first period, to 100% relative time spent in the stimulus zone in the second. Sparklines were also
162 generated to display the number of entries to each zone, and the duration of each (Figure 1A).

163 ### Shoaling cohesion assay

164 The shoaling cohesion assay apparatus was set up as described for SAZA, with the following alterations.
165 The tank had no dividing sheet, or inflow, outflow, and stimulus dispensing tubing (Figure 4A).
166 Additionally, the tracking of fish movements was not performed. To perform the assay, the tank was
167 half-filled with 20 ml of system water, then four zebrafish of 30-35 dpf were taken directly from their
168 husbandry tank and added gently to each shoaling cohesion tank. The fish were then given ~5 minutes
169 to adjust and recover post transfer until consistent swimming behaviour had resumed. Following this
170 acclimation period, 20 ml of 2x concentration alcohol solution was added to the tank to achieve the 1x
171 desired concentration for the assay. Recording began immediately and continued for 30 minutes. Six
172 repeats were performed per alcohol concentration. Following each assay, the fish were euthanized.

173 ### Shoaling cohesion data analysis

174 Video analysis was performed in imageJ. First, videos were either trimmed to the first 15 minutes, then
175 frames were extracted at 2fps to create an image stack (900 per assay), or one frame per 10 seconds of
176 footage was extracted from the full 30-minute duration (180 per assay). The image stacks for each assay
177 were cleaned using median background subtraction, then converted to 8-bit and auto-thresholded
178 (Figure 4A). From the thresholded images, particles were detected (size = 100-infinity), and the
179 centerpoint of each was determined. Using the centerpoints, Delaunay triangulation was performed on
180 each image to draw triangles covering the space between all four fish. The area of these triangles was
181 then combined to obtain the total area between the fish, as a measure of shoaling cohesion. These area

182 values were grouped into either total time for the full 30 minute duration (n = 1080 per treatment), or
183 one minute intervals for the first 15 minute data (n = 720 per time point per treatment). Values over
184 2000 $mm^2$ were identified as products of processing errors and removed (~2.5%).
185 As a measure of shoal kinesis, the distance travelled by the shoal centerpoint was calculated using the X
186 and Y coordinates for the centerpoint of the triangulation area, as calculated by imageJ, with the
187 equation; distance = $\sqrt{((X_2 - X_1)^2 + (Y_2 - Y_1)^2)}$. $X_2$ and $Y_2$ were the subsequent coordinates, 0.5s after $X_1$
188 and $Y_1$, respectively. This provided the distance the shoal centerpoint had travelled between each
189 selected frame. Values over 10 mm per 0.5s were discarded as products of processing errors, as the
190 highest velocities recorded by individual fish were ~20mm/second (Figure 3B). This amounted to < 5% of
191 the data. These values were grouped into one minute intervals for the first 15 minute data (n = 720 per
192 time point per treatment).
193

194 ## Quantitative PCR (qPCR)

195 Twelve-week old adult zebrafish were euthanized and the brains were dissected in PBS pH7.0. Brain
196 tissue was homogenised using a micro tube homogenizer (Thomas Scientific) in a lysis buffer made up of
197 Trizol (ThermoFisher #15596026). RNA was extracted using PureLink® Micro Kit (ThermoFisher
198 #K310250) according to the manufacturer's protocol. The concentration and purity of the extracted RNA
199 were determined by NanoDrop™2000 Spectrophotometer (ThermoFisher). Each brain sample yielded
200 around 100 ng/µL RNA with a ratio of absorbance reading 1.9-2.0 at 260/280 nm. The purified RNA was
201 reverse transcribed by SuperScript II First strand Synthesis System (Invitrogen #18091050) using 100
202 ng/µL of purified RNA to obtain approximately 1000 ng/µL of first strand cDNA. To check for genomic
203 DNA contamination, a negative RT (no reverse transcriptase) was set up for each sample.

204 The cDNA was diluted with nuclease-free water to 100 ng/µL. The qRT-PCR amplification mixtures (20
205 µL) contained 100 ng of cDNA, 10 µL 2x GoTaq®qPCR Master Mix (Promega #TM318), and 300 nM
206 forward and reverse primer. The primers against *chrn* targets used were designed using Primer3
207 (v.0.4.0) and are detailed in Table 3.

208 Reactions were performed using a 7500 Real-Time PCR system (Applied Biosystems) in 96-well plate
209 format. The cycling conditions were as follows: 95°C for 10m to activate the polymerase, then 40 cycles
210 of 95°C for 15s, 60°C for 30s. After completion, a melt curve was run at 65-95°C for 5 seconds per step.
211 All PCR efficiencies were above 95%. Primer specificity was validated by a single peak on the post-PCR
212 melt curve and single-band after electrophoresis.

213 The relative gene expression levels were analysed using the adjusted delta-delta CT method described
214 by Hellemans and Mortier et al. (2007). All data were analysed by one-way ANOVA, with genotype as
215 the independent variable and target gene expression, relative to reference genes, as the dependent
216 variable. For mRNA relative expression data, adjusted *p* values were estimated using Dunnett post-hoc
217 tests. Effect sizes for all differences in expression were also calculated using Cliff's Delta statistics as
218 described below.

## 219 Statistical analyses

220 Data was analysed and presented following the principles outlined by Ho *et al.* (2019), to which a p value
221 as a measure of significance is improved upon by the supplementary reporting of effect sizes, means,
222 and 95% confidence intervals (Ho et al., 2019). As the assumptions of normality and homoscedasticity
223 recommended for parametric testing could not be consistently met for the SAZA data, most unpaired
224 data were compared by non-parametric two-sided permutation T-tests, (5000 reshuffles) with a
225 significance level of 0.05, and unpaired Cliff's delta, while paired or repeated measures data were
226 compared using by paired permutation tests under the same parameters. Due to the more complex

227 design and higher replicate availability, the shoaling assay longitudinal data were analysed using a linear
228 mixed effects model, with shoal area or centerpoint travel distance as the response variable, alcohol
229 treatment and time as fixed effects, and assay ID as a random effect to account for repeated measures.
230 The residuals indicated the data were slightly skewed but appeared normally distributed and
231 homoscedastic enough to support a parametric test. Analysis was performed in R using the 'dabestr'
232 (v2024.12.24) and 'lmerTest' (v3.1-3) packages. In the case of multiple comparisons, the Holm-
233 Bonferroni step down family wise error correction was applied to the *p* value. All statistical analysis
234 outputs can be found in supplementary tables. This data was presented in the form of Gardener-Altman
235 and Cummings estimation plots. Results are reported as Cliff's delta, or Paired mean difference = X, 95%
236 CI [lower, upper], *p* = Y. For Cliff's delta, effect sizes greater than ± 0.4 and a *p*-value of < 0.01 was
237 considered meaningful and practically relevant in this study. Smaller Cliff's delta effect sizes of ± 0.2 to
238 0.4 with accompanying *p*-value of < 0.05 were also considered potentially meaningful, but provisional
239 pending experimental reproduction (Cliff, 1993; Goodman et al., 2019).

240 Hybridisation Chain Reaction, RNA-fluorescent in-situ hybridisation (HCR™ RNA-FISH)

241 Hybridisation Chain Reaction RNA-FISH 3.0 (HCR) (Choi et al. 2018) probes against *chrna3*, *chata*, and
242 *nrp1a* were prepared using an in-house Excel-based program and synthesized by IDT (please see Table 4
243 for details). The in-situ hybridization experiments were carried out in a controlled incubation chamber
244 (40°C temperature and > 90% humidity). Briefly, 14 dpf zebrafish embryos were euthanized and fixed in
245 4% formaldehyde diluted in 1X PBST at room temperature for 60 minutes with shaking. The larvae were
246 washed with 1X PBST for 3 minutes x 3 times. Embryos were permeabilized using a detergent solution
247 (1% SDS, 0.5% Tween 20, 150mM NaCl, 1mM EDTA, 0.05M Tris-HCL, pH 7.5) at 37°C for 30 minutes.
248 They were washed for 3 minutes x 3 times each with 1X PBST and then 5X SSCT. Larvae were
249 transferred to 30% probe hybridization buffer (30% formamide, 9mM citric acid, 0.1% Tween 20,

250 50µg/mL heparin, 1x Denhardt's solution, 5X SSC) and incubated at 37°C for 30 minutes. Simultaneously,
251 probes were prepared in a solution containing 30ul (10uM) of probe set against each gene in 1000 µl of
252 30% probe hybridization buffer. The larvae were either transferred to the robotic chamber or a 1.5ml
253 centrifuge tube for automated or manual experiments. Larvae were incubated with the probes at 37°C
254 for 8-12 hrs. For both methods, on day 2, larvae were washed 5 times with 30% probe wash buffer (30%
255 formamide, 9mM citric acid, 0.1% Tween 20, 50µg/mL heparin, 5x SSC) at 37°C and then 5X SSCT twice.
256 For the secondary reaction, HCR hairpins (Molecular Instruments) were diluted and prepared in an
257 amplification buffer (5X SSC, 0.1% Tween 20, 2.5% dextran sulphate) and incubated overnight (for the
258 manual methodology) or 3 hours (for the automated) in the dark. The larvae were then washed with 5X
259 SSCT, 4 X 10 mins each in the dark. They were mounted with the cover slip on the dorsal side in 70%
260 glycerol-PBS mounting media and imaged on an Olympus FV3000 confocal microscope with the settings
261 consistent between fish. Images were post-processed first on Olympus viewer FLUOVIEW FV31S-SW
262 software with linear intensity adjustments of 150 - 4095 for all genes. Images presented for *nrp1a*, *chata*
263 and *chrna3* had no further processing beyond cropping to the ROI and addition of scale bars. The *elavl3*
264 and *chrna3* false colour images were processed in Imagej. The *elavl3* images had additional linear
265 brightness/contrast adjustment (15 - 110). False colour images were converted to 8bit and had the 'fire'
266 LUT applied, followed by linear brightness/contrast adjustment of 0 - 175, background subtraction with
267 25px rolling ball, and 1px gaussian blur. Fluorescence quantification (S1, S2) was performed in ImageJ on
268 the raw images without post-processing. The regions of interest were marked using the boundaries
269 observed in *chata* for the facial motor nucleus, or *nrp1a* for the dorsal habenula, and mean grey pixel
270 value within the region was measured. Two week old (14 dpf) larvae were used for HCR imaging as this
271 age represented the upper limits of transparency without additional optical clearing steps, while being
272 closer to behavioural testing age than the traditional imaging of 5-7 dpf larvae. Single cell analysis shows

273 that 97% of the cell types in a 15 dpf fish are present in 25 dpf fish (Raj et al., 2020), so we deemed it an
274 acceptable compromise for the benefits throughput and visualisation over imaging older animals.
275

276 RNAseq

277 RNA was extracted from twelve-week old adult zebrafish *chrna3*$^{C246X}$ and WT brains in triplicate as
278 described previously. The quality of each sample was verified by gel electrophoresis and bio-analyser.
279 Samples that passed QC were sent for sequencing by Novogene AIT. An mRNA cDNA library made up of
280 Paired-end sequencing reads of 150 bp in length was generated on the Illumina HiSeq instrument. Raw
281 reads were first processed by Novogene-AIT to remove adapter, poly-N sequences, and reads with low
282 quality from raw data. All downstream analyses were based on the clean data with a Phred score of 39
283 indicating a 99.9% base call accuracy. Further analysis was performed in Partek™ Flow™ Explore Spatial
284 Multiomics Data using Partek™ Flow™ software, v11.0. Reads were aligned to GRCz11 genome assembly
285 by STAR aligner, default parameters, and subsequently filtered to a minimum mapping quality score of >
286 30. Gene counts were normalised by median ratio, followed by differential expression analysis in
287 DeSeq2. Significance thresholds were set as follows: up/down-regulated genes = $p < 0.05$ & fold change
288 > ±2. Provisional up/down-regulated genes = $p < 0.05$ & fold change < ±2. Non-significant genes = $p >$
289 0.05. Custom gene lists and sets for analysis can be found in Table 5. Gene set enrichment analysis
290 (GSEA) was performed using the GRCz11-GO database, 100 permutations. Significance thresholds were
291 set at $p < 0.05$ and FDR < 0.2. Given the loss of spatial and structural resolution when using bulk RNA
292 sequencing, this investigation was primarily targeted at identifying brain-wide, compensatory
293 mechanisms that could potentially underlie phenotypic changes, or seed predisposition to multi-
294 substance dependence and comorbid disorders, we opted for the 'fully developed' brain of the sexually

295 mature adult. These larger adult tissues provided larger quantities of high quality RNA more consistently
296 than younger animals.
297

298 # Results

299 ## Zebrafish preference for alcohol self-administration in SAZA is biphasic.

300 We refined the Self-Administration Zebrafish Assay (SAZA) first reported in (Nathan et al., 2022) to
301 improve the temporal resolution for quantifying the dynamic nature of the acute response. SAZA
302 apparatus created three chemically distinct, but physically continuous zones, or regions within the assay
303 chamber. The inflow and outflow were adjusted by gravity feed to maintain the integrity of the two
304 delivery zones throughout the assay period (Nathan et al., 2022). Subject fish behaviour was monitored
305 by a closed-loop, video acquisition program developed in-house that allowed for self-administration of a
306 stimulus or a control when subject fish entered a delivery zone from a neutral zone (Figure 1A; Movie 1).
307 To avoid intrinsically preferred swimming direction bias, the stimulus and control delivery zones were
308 pseudo-randomly assigned in each trial such that half of the fish in each group received the stimulus
309 (alcohol) in the left and the other half in the right delivery zone (Figure 1A). Sparkline plots in pilot
310 experiments showed that fish administered 20%, or 70% alcohol (at source) differentially, by changing
311 the frequency of entry, and duration of time spent in the stimulus area (Figure 1B; Movie 1). This
312 suggested that fish could quantifiably self-regulate alcohol administration, and their behaviour in the
313 closed-loop setup was dependent on stimulus concentration.

314 Next, we estimated the stimulus concentration that fish experienced during the assay. To do so, we used
315 a densitometer to measure the change in water density caused by the alcohol-water mixture. Alcohol
316 was dispensed mimicking the behaviour of fish in the pilot experiment (Figure 1B, ~10 seconds/min
317 discontinuously, table 2). This analysis revealed that, due to improved outflow and the lower density of

318 the alcohol-water mixture, the alcohol concentration in the chamber was only a fraction of that at the
319 source. This concentration was lower than previous estimates obtained from colorimetric analysis of
320 food dye-containing solution (Figure 1C). The maximum concentration plateaued at ~40-fold lower than
321 the source alcohol concentration, which was at least four-fold lower than previous studies (Nathan et
322 al., 2022). Therefore, on an average, self-administering source alcohol at 20% and 70% resulted in the
323 fish experiencing alcohol at ~0.5% and ~1.5% respectively in the assay (Figure 1C; for 20%, $\bar{x}$ = 0.52 %, SD
324 = 0.13%; 70%, $\bar{x}$ = 1.52%, SD = 0.44%). We refer to these two conditions as $\bar{x}$0.5% condition and $\bar{x}$1.5%
325 respectively in the rest of this study. The effective concentration reduced by half within a minute of
326 stopping self-administration (Figure 1C). Thus, both the pre, and post-administration periods served as
327 controls to compare the behaviour of animals in the naïve pre, and post exposure periods. This range of
328 alcohol exposure is comparable to the concentration of alcohol used in previous zebrafish studies (Kurta
329 and Palestis, 2010; Echevarria et al., 2011; Mathur et al., 2011; Tsang et al., 2019).

330 The dynamic change in alcohol concentration over time during SAZA is a key advantage for untangling
331 the small effects single genes may have on complex behaviours like alcohol preference. Common
332 variants in *CHRNA3*, for example, are risk factors for developing nicotine dependence, while several rare
333 variants are proposed to influence cocaine and alcohol dependence (Haller et al., 2014; Kamens et al.,
334 2023). *Chrna3* is proposed to mediate alcohol stimulant effects in rodents (Kamens et al., 2009).
335 However, this gene's role in development of alcohol dependence hasn't been tested directly. We
336 hypothesised that the SAZA will be effective in examining such a role, if present, in nicotinic
337 acetylcholine receptor alpha3 (*chrna3)* mutant generated recently (Kibat, 2020).

338 The *chrna3* mutant harbours an insertion that causes a frameshift and introduces a premature stop
339 codon within transmembrane domain 1 of the gene, resulting in a truncated protein at amino acid
340 position 246 (*chrna3*$^{C246X}$; Figure 1D). The mutant protein is predicted to have a large truncation of the
341 transmembrane and the intracellular domains (Figure 1E) and is thus expected to be damaging to

342 protein function. Quantitative RT-PCR of adult whole brains showed that the mutation resulted in a
343 significant reduction in the expression of *chrna3* transcripts in the mutants (Figure 1F, *WT* vs.
344 *chrna3*$^{C246X}$, Cliff's delta = -0.848, 95CI [-0.567, -0.962], $p$ = < 0.001). In rodents, *Chrna3* expression is
345 restricted. It is expressed in a few neurons in the hippocampus, medial habenula, interpeduncular
346 nucleus (IPN), the ventral tegmental area (VTA), cerebellum, locus coeruleus, and spinal cord (Wada et
347 al., 1989; Gotti et al., 2006). We investigated the expression of *chrna3* in 14 days post fertilization (dpf)
348 zebrafish larvae using an in-house modified Hybridisation Chain Reaction™ RNA fluorescence in-situ
349 hybridisation (HCR) method (Banerjee et al., 2024). As cholinergic function in the hindbrain motor
350 neurons and expression in facial motor nucleus (Fmn) have also been previously reported (Rima et al.,
351 2020), we quantified *chrna3* expression in the mutants. While expression of *chrna3* was high in the wild
352 types, it was starkly and consistently reduced in the mutants (Figure 1G, S1). We also examined
353 expression of *chrna3* in brain regions such as the medial habenula (dorsal habenula in zebrafish),
354 reported to have co-expression of *CHRNA5-A3-B4* in mammals (Xu et al., 2006; Fowler et al., 2011). Only
355 a few cells in the left dorsal habenula expressed *chrna3* at a low level. The expression levels in the
356 mutant and WT were similarly low (Figure 1H, S2).
357
358 Having established a robust system for quantifying self-administration and generated *chrna3*$^{C246X}$
359 mutants, we examined the behaviour of juvenile fish in the SAZA at an age when they show consistency
360 across the population (~5 weeks old). We first examined the response of wild-type animals (WT). The
361 pilot (Figure 1B) suggested the preference changed dynamically over the course of the assay. To capture
362 this, we collapsed the preference behaviour of animals over 3-minute windows that balanced temporal
363 granularity in relation to the changing alcohol concentration with quantifiable observation periods. The
364 preference was unchanged over time when alcohol was absent (0%; Figure S3). The same analysis for
365 the x̄0.5% alcohol condition revealed that fish initially spent significantly more time in the stimulus zone

366 compared to the pre-exposure period (Figure 2A, 3-6m, Paired mean difference = 7.62, 95CI [13.9,
367 0.331], $p_{adj}$ = 0.028). However, after about 10 minutes, fish reversed their preference and spent
368 significantly less time in the stimulus zone (Figure 2A, 12-15m, Paired mean difference = -6.47, 95CI [-
369 2.2, -10.1], $p_{adj}$ = 0.031). This avoidance continued for the remainder of the assay, even after the self-
370 administration period ended. However, the early attractive portion of this biphasic response was absent
371 in the x̄1.5% condition (Figure 2B, 3-6m, Paired mean difference = -1.1, 95CI [4.26, -6.27], $p_{adj}$ = 1). Fish
372 spent less time in the stimulus zone from six minutes onwards (Figure 2B, 6-9m, Paired mean difference
373 = –8.57, 95CI [-3.22, -13.00], $p$ = 0.012). Mapping the behavioural changes to the alcohol concentration
374 expected in the stimulus zone revealed that juvenile zebrafish preferred alcohol when the concentration
375 was under 0.5%, while they avoided ~0.7% or higher alcohol (Figure 2C). Thus, WT zebrafish self-
376 regulated alcohol exposure within a narrow range.

377

378 *chrna3* mutant fish show higher tolerance to alcohol

379 We next examined the behaviour of *chrna3*$^{C246X}$ mutants in the SAZA. Mutants, similar to WT
380 counterparts showed no preference in the absence of alcohol (0%; Figure S3, A-B). In the x̄0.5%
381 condition, *chrna3*$^{C246X}$ fish initially behaved like their WT spending significantly more time in the stimulus
382 zone (Figure 2D, 3-6m, Paired mean difference = 13.9, 95CI [20.3, 8.18], $p_{adj}$ = 0.005). However, unlike
383 the WT, this attraction persisted throughout the assay period (Figure 2D, 9-12m, Paired mean difference
384 = 5.96, 95CI [10.1, 1.94], $p_{adj}$ = 0.044). No biphasic switch to avoidance was observed. Surprisingly,
385 mutants did not show a strong avoidance response during the assay even in the x̄1.5% condition (Figure
386 2E, 12-15m, Paired mean difference = -7.15, 95CI [-1.13, -12.4], $p_{adj}$ = 0.134).

387 The total time spent in the control delivery zone varied among conditions and genotype, but did not
388 show a consistent trend (Figure S3, C-H). The frequency of entry into the stimulus zone however, was
389 correlated with the time spent in the stimulus zone. This was similar across both genotypes in the x̄0.5%

390 condition and was indicative of the preference behaviour seen (Figure S4, C-D). Interestingly, the
391 frequency of entry into the stimulus zone in the x̄1.5% condition showed a brief increase initially across
392 the two genotypes (0-3 mins; Figure S4, E-F), before it plateaued off to pre-stimulus frequency rapidly,
393 suggesting that a reduction in total time spent in the stimulus zone observed in Figure 2B and 2E was
394 driven by shorter visits, rather than reduced frequency of visits.
395
396 Despite the early attraction (Figure 2A, 2D), in general alcohol appeared to be aversive to WT zebrafish
397 albeit less so for the mutants. This could also be inferred from the volumes delivered in alcohol
398 conditions compared to the volumes delivered in the 0% alcohol condition (Figure 3A, 3B). WT fish self-
399 administered significantly smaller volumes in the x̄0.5% condition (Figure 3A, Cliff's delta = -0.554, 95CI
400 [-0.266, -0.759], $p_{adj}$ = <0.001), and in the x̄1.5% condition (Figure 3A, Cliff's delta = -0.728, 95CI [-0.441,
401 -0.895] $p_{adj}$ = <0.001). This supports previous observations that alcohol can be aversive to zebrafish at
402 certain concentrations (Nathan et al., 2022). The *chrna3*$^{C246X}$ mutant fish however, reduced volume of
403 administration only in the x̄1.5% condition (Figure 3B, 0% vs x̄1.5%, Cliff's delta = -0.583, 95CI [-0.304, -
404 0.791], $p_{adj}$ = < 0.001), and the two genotypes differed only during the x̄0.5% condition (Figure 3C, x̄0.5%,
405 Cliff's delta = -0.328, 95CI [0.584, 0.009], $p_{adj}$ = 0.027).
406 To quantify the magnitude of the difference between genotypes we examined a Preference Index (PI;
407 see methods). PI was calculated for each subject as the relative preference for the stimulus compared to
408 control. Positive PI values (0 to +1) therefore indicated a preference for stimulus, while negative values
409 (0 to -1) indicated an aversion. We also quantified a delta, or the change in the PI itself in subsequent
410 phases: pre-exposure phase, the early phase (0-9 minutes), and the late phase (9-18 minutes). The
411 duration of the phases coincides with the time required (~10 minutes) for equilibration of blood alcohol
412 concentration in larvae immersed in alcohol (Lockwood et al., 2004). We used the "delta-delta", or the

413 difference of this measure between the two genotypes to quantify what aspect *chrna3* contributes to
414 most (Figure 3).

415 As anticipated, the PI range was broad, and population mean was centred around zero in the 0% alcohol
416 condition (Figure 3D). No significant change was observed between pre and early phases for either
417 genotypes. Consequently, the delta-delta between genotypes was also insignificant (Figure 3D).
418 However, both WT and mutants showed a positive preference shift in the early phase in the x̄0.5%
419 condition (Figure 3E, WT, Paired mean difference = 0.181, 95CI [0.321, 0.017], $p_{adj}$ = 0.036, Figure 3E,
420 *chrna3*$^{C246X}$ , Paired mean difference = 0.34, 95CI [0.488, 0.232], $p_{adj}$ = < 0.001). The delta-delta between
421 genotypes changed only marginally (Figure 3E). The genotypic however, was significantly different in the
422 x̄1.5% SAZA (Figure 3F, Delta-Delta = 0.305, 95CI [0.478, 0.114], $p_{adj}$ = 0.009). In the second half of the
423 SAZA self-administration period, once again the 0% condition had no directional change between the
424 phases, or the genotypes (Figure 3G). Although both genotypes showed similar trend in the x̄0.5%
425 condition (Figure 3H), it was notable that the individual variance in the PI was small for mutants, while it
426 was considerably broader for WT, distributed across preference and aversion. Finally, in the x̄1.5%
427 condition, the PI shifted towards aversion, or negative values substantially for WT (Figure 3I, WT, Paired
428 mean difference = -0.3, 95CI [-0.144, -0.462], $p_{adj}$ = 0.001). One the other hand, the PI in the mutants
429 showed no directionality (Figure 3I). In addition to this increased alcohol tolerance in the x̄1.5%
430 condition the mutants also exhibited heightened alcohol-induced locomotor stimulation over the full
431 stimulus-dispensing period (x̄0.5% condition; Figure S5, A-F) that impacted other behavioural
432 characteristics of the mutants (Figure S6). Altogether, this suggested that manipulation of *chrna3*
433 function exerted larger effects on the alcohol tolerance at higher alcohol concentrations than impact the
434 attractive response at lower concentrations.

435

436 Shoaling behaviour shows biphasic effects of alcohol exposure.

437 We next explored the potential reasons for this rapid and biphasic response to alcohol self-
438 administration. Alcohol is well-documented to act as an anxiolytic, reducing a variety of anxiety-like
439 behaviours in fish (Gebauer et al., 2011; Araujo-Silva et al., 2020). However, it is also known to function
440 as a sedative, causing reduced swimming velocity and coordination, and increased immobility
441 (Echevarria et al., 2011; Tsang et al., 2019). We hypothesised that the biphasic response in SAZA is
442 correlated to the concentrations at which these two contrasting effects of alcohol come into play. To
443 test this, we examined the shoaling behaviour of juvenile fish. Shoal members are proposed to swim
444 near others when anxious and are expected to be more exploratory when the anxiety-like state is
445 reduced (Miller et al., 2013), for example under an anxiolytic alcohol dose. This will be reflected by an
446 increase in the total area occupied by the shoal, or decreased shoal cohesion. On the other hand, shoal
447 members experiencing the sedative effects of alcohol are expected to swim with decreased speed and
448 coordination. This impacts the distance travelled by the shoal, or the shoal kinesis, in addition to
449 reducing the shoal cohesion. Hence, the impact of both the anxiolytic and sedative effects of alcohol can
450 be measured by examining shoal cohesion and kinesis in tandem (Figure 4A). Shoal cohesion was
451 quantified by defining each fish as a point, then triangulating the lines between them to give the total
452 area between fish. Shoal kinesis was calculated by the distance between the shoal centre points, as
453 defined by the crossing point of the triangulation between fish, between frames at 2fps (Figure 4A).

454 Taking into account the concentrations associated with attraction and aversion (Figure 2C), we
455 examined the shoaling behaviour of four fish over 30 minutes at two fixed concentrations of 0.5%, or 1%
456 alcohol and compared their behaviour when alcohol was absent (0%; Figure 4A, Movie 2). The total area
457 between WT shoal members increased at both concentrations, with the 1% alcohol having a
458 proportionally larger effect on the shoal area (Figure 4B, 0 vs 0.5%, Cliff's delta = 0.409, 95CI [0.453,
459 0.364], $p_{adj}$ = < 0.001, 0 vs 1%, Cliff's delta = 0.518, 95CI [0.559, 0.475] $p_{adj}$ = < 0.001). The same

460 phenomenon was also observable in the mutants (Figure 4C, 0 vs 0.5%, Cliff's delta = 0.365, 95CI [0.412,
461 0.320], $p_{adj}$ = < 0.001, 1%, Cliff's delta = 0.611, 95CI [0.649, 0.573] $p_{adj}$ = < 0.001).
462 Differences between the two genotypes emerged when their behaviours were examined at a higher
463 temporal resolution. Loss of cohesion in WT fish was observable within five minutes of exposure to
464 either concentration (Figure 4D, 0 vs 0.5% 3-6m, Cliff's delta = 0.287, 95CI [0.320, 0.252], $p_{adj}$ = 0.032;
465 Figure 4D 0 vs 1% 3-6m, Cliff's delta = 0.338, 95CI [0.370, 0.305], $p_{adj}$ = 0.004). The magnitude of the
466 difference increased over time (Figure 4D, 0 vs 0.5% 12-15m, Cliff's delta = 0.552, 95CI [0.579, 0.522],
467 $p_{adj}$ = < 0.001; 0 vs 1% 12-15m, Cliff's delta = 0.728, 95CI [0.749, 0.707], $p_{adj}$ = < 0.001). Shoal kinesis
468 changed negligibly over time with 0.5% alcohol treatment, while it was reduced almost immediately
469 with 1% alcohol treatment. The effect became larger over time (Figure 4E, 0 vs 1%, 6-9m, Cliff's delta = -
470 0.419, 95CI [-0.387, -0.449], $p_{adj}$ = 0.001). Thus, immersion in 0.5% alcohol reduced anxiety-like
471 behaviours, while sedative-like effects were more evident when immersed in 1% alcohol (Figure 4D, 4E).
472 The *chrna3*$^{C246}$ mutants seemed to experience the effects of alcohol exposure differently. Behaviour of
473 unexposed (0% alcohol) was similar between the two genotypes with the *chrna3*$^{C246X}$ exhibiting only
474 slight differences in shoal cohesion (Figure S7, A), and shoal kinesis (Figure S7B). However, unlike the WT
475 shoals, exposure to 0.5% alcohol reduced shoal cohesion only marginally (Figure 4F) and it did not
476 increase over time as it did in the WTs (Figure 4D). This difference is clearer when genotypes are
477 compared directly. Mutant fish retained significantly tighter shoaling cohesion compared to the wild
478 type (Figure 4H, 12-15m, Cliff's delta = -0.44, 95CI [-0.409, -0.47], $p_{adj}$ = < 0.001). Meanwhile, shoal
479 kinesis was initially heightened in *chrna3*$^{C246X}$ fish compared to the WTs (Figure 4I, 0-3m, Cliff's delta =
480 0.253, 95CI [0.288, 0.219], $p_{adj}$ = 0.004), which paralleled the *chrna3*$^{C246X}$ alcohol-induced motility
481 stimulation in the SAZA (Figure S5, A-F). The alcohol-induced kinesis difference between genotypes
482 gradually declined as the assay progressed (Figure 4I). This divergence in behaviours between genotypes

483 suggests that the anxiolysis from the alcohol exposure was much lower in *chrna3*$^{C246X}$ than that
484 experienced by their WT counterparts.

485 The behaviour differences between the mutant and wild-type shoals were minimal in 1% alcohol for the
486 majority of the assay duration (Figure S7, C-D). However, in the latter part of the assay mutants seemed
487 to resist the sedative effects of alcohol, retaining higher shoal kinesis than the wild type (Figure S7D, 15-
488 18m, Cliff's delta = 0.372, 95CI [0.405, 0.34], $p_{adj}$ = 0.008). The effects of alcohol on shoal cohesion and
489 kinesis in the first five minutes of exposure were similar between genotypes (Figure 4, S7). Overall, these
490 results from the shoaling assay suggest that *chrna3*$^{C246X}$ had reduced effect of alcohol exposure on
491 anxiolysis as well as sedative effects seen in WT fish.

492

493 Whole brain transcriptomic analysis shows major neurotransmitter signalling pathways are affected in
494 mutants

495 To gain an understanding of these behavioural differences we performed bulk RNA sequencing of WT
496 and mutant whole brains. Differential gene expression (DEG) analysis suggested that the two genotypes
497 had large differences, with PC1 accounting for ~44% of the variation in a PCA (Figure 5A). Gene Set
498 Enrichment Analysis (GSEA) revealed notable enrichment in transcriptional changes in mutants (Figure
499 5B). The significantly enriched biological functions impacted in the mutant included neuronal
500 development, ion channel function, and secondary messenger-associated processes (Figure 5B).
501 Additionally, genes associated with feeding behaviour were also enriched. In total, the expression of
502 ~1600 genes was significantly changed (2-fold or more), and a further ~4600 genes were identified with
503 provisional alterations (less than 2 fold; Figure 5C). Of these, there was an approximately even split
504 between up- and down-regulated gene numbers (Figure 5C). Together, this perhaps indicates a wide
505 cascade of compensatory changes induced by the reduced expression and function of *chrna3.*

506 Major neurotransmitter signalling including glutamate, and GABA receptors in addition to nAChRs,
507 which are activated by exposure to psychoactive substances like alcohol, also showed modest changes
508 in expression patterns (Figure 5D-F). Both glutamate and GABA receptors appeared to show a small but
509 consistent upregulation amongst many receptor subunits (Figure 5D-E). The expression of most nAChR
510 genes however was unchanged, though a few were positively or negatively regulated with no consistent
511 trend (Figure 5F). Closer inspection of the nAChR subunit gene counts revealed that expression was very
512 low for some subunits, as was highlighted for *chrna3* in the HCR (Figure 1, 5G). For genes with low
513 expression counts it is a challenge to determine significant changes through RNA-seq analysis. As
514 *CHRNA3* expression is co-regulated with *CHRNA5* and *CHRNB4* in humans, both of which have also been
515 associated with substance use disorders (Wen et al., 2016), we examined whether the expression of
516 these genes had also been altered in the mutant. Both *chrna5* and *chrnb4* displayed significant
517 downregulation by qPCR, with the effect size being much larger for the latter (Figure 5H).
518 We also examined gene sets curated from meta-analyses of genes consistently associated with alcohol
519 and nicotine dependence in humans (Hu et al., 2018), and with mammalian anxiety phenotypes (Howe
520 et al., 2016; Koskinen and Hovatta, 2023) to address whether *chrna3* dysfunction also alters expression
521 of these genes (Figure 5I-K). The alcohol dependence-associated genes exhibited few changes (Figure
522 5I), however, ~50% of the nicotine-dependence genes were provisionally upregulated in the mutant
523 (Figure 6J). Finally, genes associated with anxiety phenotypes also showed a number of expression
524 changes, albeit some in positive and some in negative direction of expression (Figure 5K). In all cases,
525 this analysis revealed that though the expression of a large number of these genes changed they were
526 modest.
527

528 ## Discussion

529 In this study, a refinement of self-administration zebrafish assay (SAZA) revealed an acute biphasic
530 response to alcohol, in juvenile zebrafish, with preference transitioning to avoidance when exposure
531 increased to ~0.7% alcohol (Figure 2). This biphasic response to alcohol aligns zebrafish with other
532 animals, suggesting that hormesis to alcohol is a fundamental property across vertebrates (Figures 1, 2;
533 (Calabrese and Baldwin, 2003; Calabrese, 2008; Sterling et al., 2015)). The closed-loop design of SAZA,
534 similar to a two-bottle choice assay used for rodents, facilitated the analysis of uninhibited choice and
535 isolated *chrna3*'s role in modulating this biphasic response.

536 Isolating contributions of individual genetic factors to a phenomena such as substance dependence is
537 challenging. It is further compounded for multi-subunit receptor genes that cluster at a genomic locus,
538 such as the *CHRNA5-A3-B4* gene cluster. This genomic locus has been consistently associated with
539 several substance use disorder GWASes (Chen et al., 2009; Maes et al., 2011; Haller et al., 2014; Wen et
540 al., 2016). Although, male transgenic mice overexpressing *Chrna5-a3-b4* consume less alcohol than wild-
541 type mice (Gallego et al., 2012), a causal relationship can't be ascribed to *Chrna3* alone from this study
542 (Kamens et al., 2023). *Chrna3* knockout mice die prematurely as neonates (Xu et al., 1999) and the
543 conditional knockout (Elayouby et al., 2021) only examined nicotine response leaving the role of α3 in
544 alcohol stimulation unclear (Kamens et al., 2009). Zebrafish *chrna3* mutants, however, survive to
545 adulthood, offering a tractable system to investigate gene-specific effects here. *chrna3* mutants
546 displayed a blunted aversive switch in the biphasic response, while maintaining early attraction (Figure
547 2, 3). WT fish exhibited aversive behaviour to 0.7% or higher alcohol stimulus, which only became
548 observable in mutants at higher concentrations. This aligns with rodent studies, where a broad spectrum
549 nicotinic receptor antagonist 18-MC in the medial habenula (MHb) - interpeduncular nucleus (IPN)
550 circuit reduced transmission and increased nicotine or alcohol self-administration, respectively (Glick et
551 al., 2011; Miller et al., 2019). As this circuit co-expresses all the three nAChR subunits α3, α5, and β4,

552 they are thus proposed to mediate aversion to psychoactive substances, including alcohol (Marks et al.,
553 1992; Xu et al., 2006; Frahm et al., 2011; Fowler and Kenny, 2012; Mathuru, 2018; Elayouby et al., 2021).
554 However, as shown in the gene expression profile here (Figure 1), and in a recent report (Hua et al.,
555 2025), *chrna3* is expressed widely in the central and peripheral nervous system. Consequently, altered
556 alcohol tolerance reported here may stem from a combined effect across multiple circuits and systems.
557 Further to this limitation, although most physiological features and brain regions described in adult
558 zebrafish are present in juveniles by 25 dpf, late-stage developmental changes may influence adult
559 phenotypes (Schmidt et al., 2013; Singleman and Holtzman, 2014; Raj et al., 2020), warranting further
560 studies.

561 A shifted tolerance window exhibited by *chrna3* mutants (Figure 3C) suggests a threshold based
562 engagement of different brain circuits, similar to the proposed mammalian twin threshold model
563 (Grasing, 2016). This model posits that cholinergic signalling, particularly in the VTA and nucleus
564 accumbens (NAc), modulates drug reinforcement behaviours. In this model, lower threshold increases
565 positive reward association probability, stimulating behavioural repetition, while a second, higher
566 threshold does the opposite as different circuits come into play (Grasing, 2016). This may also be
567 applicable to other cholinergic brain regions, such as the MHb. Additionally, higher agonist requirements
568 to activate α5, α3, and β4 containing nAChRs (Coe et al., 2005), could elevate the cholinergic threshold
569 to engage this aversive circuit, providing a potential explanation for why *chrna3* mutation
570 predominantly affected the avoidance response.

571 Beyond preference, *chrna3* mutation also blunted the psychoactive effects of alcohol during immersion.
572 Immersion is a rapid, non-invasive route for administration of water-soluble pharmaceutics, uniquely
573 available for aquatic animals. Alcohol immersion time correlates with blood alcohol concentration (BAC)
574 until equilibrium is reached, and is a key measure affecting physiological responses (Lockwood et al.,
575 2004). As in humans, BAC > 0.05%, or the equivalent of ~2-3 Australian "standard drinks", results in

576 significant behavioural impairment in zebrafish, which can be reached within 1-2 minutes of immersion
577 in 1.5% alcohol. This manifests in humans as slower reaction times (Grant et al., 2000), and zebrafish as
578 loss of swimming coordination or impaired locomotion (Tran and Gerlai, 2013; Tsang et al., 2019).
579 However, lower concentrations are stimulatory, activating dopaminergic reward pathways and
580 increasing locomotion, while reducing anxiety-like behaviours and aggression (Echevarria et al., 2010;
581 Araujo-Silva et al., 2020).

582 Shoaling behaviour, that becomes prominent by 14 dpf (Miller and Gerlai, 2007), can effectively model
583 these contrasting effects (Oscar-Berman and Marinković, 2007; Kurta and Palestis, 2010; Miller et al.,
584 2013; Rueger and King, 2013) at SAZA-relevant concentrations. In wild types, both 0.5% and 1% alcohol
585 immersion gradually reduced shoal cohesion, but exhibited differing effects on shoal kinesis (Figure 4).
586 One interpretation of the coupled reduction in cohesion and kinesis in 1% alcohol is as a sedative effect,
587 evident also in the video recordings (Movie 2). Meanwhile, reduction of cohesion alone could indicate
588 an anxiolytic effect, that dominated in a narrow alcohol concentration range (0.5%). These
589 concentrations approximately correlated with the attractive and aversive doses during SAZA, suggesting
590 a potential link. However, the *chrna3*$^{C246X}$ mutants displayed no reduction in shoal cohesion at 0.5%
591 (Figure 4H). Whether this reduction in anxiolysis phenotype in the mutants was directly due to reduced
592 sensitivity to alcohol or independent of it needs further investigation. Irrespective, it is evident that the
593 *chrna3* mutation blunted drug-induced behavioural effects, including the reduced aversion in SAZA.

594 Alcohol-induced kinesis also differed between genotypes, with *chrna3*$^{C246X}$ mutants exhibiting stronger
595 alcohol-induced locomotion in SAZA and shoaling assays (Figure 4, S5). This may be correlated to the
596 reduced expression of *chrna3* in the caudal and rostral regions of the mutant facial motor nucleus
597 (Fmn), also termed the octavolateral efferent nucleus (OEN) (Figure 1, S1), a hindbrain region connected
598 to the lateral line. Cholinergic signalling here is hypothesised to act as a 'brake' on locomotor auto-
599 sensory stimulation generated during swimming (Pichler and Lagnado, 2020; Manuel et al., 2021;

600 Odstrcil et al., 2022). While typically this function is assigned to α9 receptors, if α3 plays a role, as
601 suggested recently (Rima et al., 2020), it may account for the heightened alcohol-induced locomotor
602 response in *chrna3*$^{C246X}$ mutants. However, *chrna3*'s influence on locomotor control requires further
603 investigation, as rodent studies offer inconsistent evidence (Kamens et al., 2009).

604 Whole-body mutation in our *chrna3* mutant precluded implicating specific brain regions like the dorsal
605 habenula (MHb in mammals), yet, it does inform on potential consequences of *CHRNA3* variants that
606 reduce α3 function in humans. Whole brain RNA sequencing identified broad transcriptional profile
607 change in the mutants. Small, but, consistent upregulation of nicotine dependence associated genes was
608 indicative of a bi-directional relationship (Figure 5J; (Hu et al., 2018)), aligning with GWAS studies linking
609 *CHRNA3* polymorphisms to increased nicotine dependence (Chen et al., 2009; Maes et al., 2011).
610 Downregulation of *chrna5* and *chrnb4* (Figure 5H), also associated with substance dependence (Fowler
611 et al., 2011; Frahm et al., 2011) and co-expressed with *chrna3* in other vertebrates, potentially
612 contributed to the mutant's alcohol tolerance. Generation and characterization of an independent
613 *chrna3*, *chrna5,* and *chrnb4* mutant lines along with their combinations (currently in progress), will be
614 invaluable to dissociate these factors further.

615 Beyond nAChRs, alcohol impacts both glutamate and GABA receptors, modulating excitatory and
616 inhibitory tones, respectively (Davies, 2003; Möykkynen and Korpi, 2012; Jones, 2019). Consequently,
617 changes in expression of these receptor genes (Figure 5D, 5E) in mutants was also interesting to
618 observe, as many homologs also feature in nicotine dependence and anxiety phenotypes in humans
619 (Figure 5J, 5K). At a functional level, neuronal receptor related GO terms like synaptic signalling, ion
620 channel function, and cation homeostasis were significantly enriched (Figure 5B). However, neural
621 development terms including neuron projection, dendrite development, and axon guidance were also
622 enriched despite the use of adult brains (Figure 5B), perhaps indicative of compensatory plasticity.
623 Finally, enrichment of feeding behaviour associated genes was notable (Figure 5B), as cholinergic

624 signalling and CHRNA5-CHRNA3-CHRNB4 cluster SNPs have been tentatively linked by GWAS studies to
625 smoking/obesity interactions (Varga et al., 2013; Herman et al., 2016; Ortiz-Guzman et al., 2024). This
626 transcriptomic change warrants further examination to determine the simultaneous influence of *chrna3*
627 on substance dependence and other comorbid disorders.

628 Overall, these findings suggest the type of brain-wide compensatory changes that may occur
629 corresponding to loss of *chrna3* function, eventually resulting in heightened alcohol tolerance and
630 potential predisposition to multi-substance use and comorbid disorders.

631 Understanding alcohol's biphasic properties is imperative to address Alcohol Use Disorder (AUD). Our
632 study fills a gap, providing novel evidence on the role of *chrna3* in modulating alcohol preference, and
633 tethering it to a specific facet of the dose-response curve. Given the paucity of animal model data,
634 despite GWAS associations (Haller et al., 2014), the evidence of isolated gene function from a whole
635 body mutation in zebrafish presented here represents a valuable step forward in the context of
636 phenotypes leading to alcohol dependence development in humans harbouring *CHRNA3* variants.

637

638

## Acknowledgements:

We would like to thank the zebrafish fish facility (ZFF) staff at the IMCB, A*STAR for their assistance with fish husbandry. We also thank Li Xinrui for generating customized Python analysis scripts. Additionally, during the preparation of this work the author(s) used Grammarly, and Gemini in order to assist with grammar and consistency of phrasing. After using this tool/service, the author(s) reviewed and edited the content as needed and take(s) full responsibility for the content of the publication.

## Supplementary Materials:

Supplementary Material Figures S1 to S7, Tables S1 to S3.

Number of supplementary figures and tables = 10

## Author Contributions:

Conceptualization, A.S.M, and J.R; methodology, A.S.M., T.D.B., C.K., and J.R.; formal analysis, J.R., T.D.B and A.S.M.; investigation, J.R., C.K., and A.S.M; resources, A.S.M; writing—original draft preparation, J.R, and A.S.M.; writing—review and editing, All.; visualisation, J.R.; supervision, A.S.M.; project administration, A.S.M., A.M.; funding acquisition, A.S.M.

## Funding:

This research was funded by the Ministry of Education (MOE), Singapore (through grant number T2EP30220-0020), and Yale-NUS College (through grant numbers IG16-LR003, IG18-SG103, IG19-BG106, and SUG) to ASM.

## Data Availability Statement:

The datasets used to generate the figures are included within the article and its additional file(s). Additional data are available from the corresponding author upon request.

## Conflicts of Interest:

The authors declare no conflict of interest. The sponsors had no role in the design, execution, interpretation, or writing of the study.

666 ## References


667 Amos CI, Spitz MR, Cinciripini P (2010) Chipping away at the genetics of smoking behavior. Nat Genet
668 42:366–368.

669 Araujo-Silva H, Leite-Ferreira ME, Luchiari AC (2020) Behavioral Screening of Alcohol Effects and
670 Individual Differences in Zebrafish (Danio rerio). Alcohol Alcohol 55:591–597.

671 Aslam A, Kwo PY (2023) Epidemiology and Disease Burden of Alcohol Associated Liver Disease. J Clin Exp
672 Hepatol 13:88–102.

673 Banerjee TD, Raine J, Mathuru AS, Chen KH, Monteiro A (2024) Spatial mRNA profiling using Rapid
674 Amplified Multiplexed-FISH (RAM-FISH). bioRxiv:2024.12.06.627193 Available at:
675 https://www.biorxiv.org/content/10.1101/2024.12.06.627193v1.abstract [Accessed May 5, 2025].

676 Bassett AR, Tibbit C, Ponting CP, Liu J-L (2013) Highly efficient targeted mutagenesis of Drosophila with
677 the CRISPR/Cas9 system. Cell Rep 4:220–228.

678 Bierut LJ (2011) Genetic vulnerability and susceptibility to substance dependence. Neuron 69:618–627.

679 Bogdan R, Hatoum AS, Johnson EC, Agrawal A (2023) The Genetically Informed Neurobiology of
680 Addiction (GINA) model. Nat Rev Neurosci 24:40–57.

681 Bossé GD, Peterson RT (2017) Development of an opioid self-administration assay to study drug seeking
682 in zebrafish. Behav Brain Res 335:158–166.

683 Calabrese EJ (2008) U-shaped dose response in behavioral pharmacology: historical foundations. Crit
684 Rev Toxicol 38:591–598.

685 Calabrese EJ, Baldwin LA (2003) Ethanol and hormesis. Crit Rev Toxicol 33:407–424.

686 Chen X, Chen J, Williamson VS, An S-S, Hettema JM, Aggen SH, Neale MC, Kendler KS (2009) Variants in
687 nicotinic acetylcholine receptors alpha5 and alpha3 increase risks to nicotine dependence. Am J
688 Med Genet B Neuropsychiatr Genet 150B:926–933.

689 Chvilicek MM, Titos I, Rothenfluh A (2020) The Neurotransmitters Involved in Alcohol-Induced
690 Behaviors. Front Behav Neurosci 14:607700.

691 Cliff N (1993) Dominance statistics: Ordinal analyses to answer ordinal questions. Psychol Bull 114:494–
692 509.

693 Coe JW et al. (2005) Varenicline: an alpha4beta2 nicotinic receptor partial agonist for smoking cessation.
694 J Med Chem 48:3474–3477.

695 Cox TC (2015) Utility and limitations of animal models for the functional validation of human sequence
696 variants. Mol Genet Genomic Med 3:375–382.

697 Cully M (2019) Zebrafish earn their drug discovery stripes. Nat Rev Drug Discov 18:811–813.

698 Davies M (2003) The role of GABAA receptors in mediating the effects of alcohol in the central nervous
699 system. J Psychiatry Neurosci 28:263–274.

700 de Magalhães JP (2015) The big, the bad and the ugly: Extreme animals as inspiration for biomedical
701 research. EMBO Rep 16:771–776.

702 Echevarria DJ, Hammack CM, Jouandot DJ, Toms CN (2010) Does Acute Alcohol Exposure Modulate
703 Aggressive Behaviors in the Zebrafish (Danio rerio), or is the Bark Worse than the Bite? Int J Comp
704 Psychol 23 Available at: https://escholarship.org/content/qt2px3t3jc/qt2px3t3jc.pdf?t=mwj0ph
705 [Accessed October 20, 2023].

706 Echevarria DJ, Toms CN, Jouandot DJ (2011) Alcohol-induced behavior change in zebrafish models. Rev
707 Neurosci 22:85–93.

708 Egervari G, Siciliano CA, Whiteley EL, Ron D (2021) Alcohol and the brain: from genes to circuits. Trends
709 Neurosci 44:1004–1015.

710 Elayouby KS, Ishikawa M, Dukes AJ, Smith ACW, Lu Q, Fowler CD, Kenny PJ (2021) α3* Nicotinic
711 Acetylcholine Receptors in the Habenula-Interpeduncular Nucleus Circuit Regulate Nicotine Intake.
712 J Neurosci 41:1779–1787.

713 Fowler CD, Kenny PJ (2012) Habenular signaling in nicotine reinforcement. Neuropsychopharmacology
714 37:306–307.

715 Fowler CD, Lu Q, Johnson PM, Marks MJ, Kenny PJ (2011) Habenular α5 nicotinic receptor subunit
716 signalling controls nicotine intake. Nature 471:597–601.

717 Frahm S, Slimak MA, Ferrarese L, Santos-Torres J, Antolin-Fontes B, Auer S, Filkin S, Pons S, Fontaine J-F,
718 Tsetlin V, Maskos U, Ibañez-Tallon I (2011) Aversion to nicotine is regulated by the balanced activity
719 of β4 and α5 nicotinic receptor subunits in the medial habenula. Neuron 70:522–535.

720 Gallego X, Ruiz-Medina J, Valverde O, Molas S, Robles N, Sabrià J, Crabbe JC, Dierssen M (2012)
721 Transgenic over expression of nicotinic receptor alpha 5, alpha 3, and beta 4 subunit genes reduces
722 ethanol intake in mice. Alcohol 46:205–215.

723 Gebauer DL, Pagnussat N, Piato AL, Schaefer IC, Bonan CD, Lara DR (2011) Effects of anxiolytics in
724 zebrafish: similarities and differences between benzodiazepines, buspirone and ethanol. Pharmacol
725 Biochem Behav 99:480–486.

726 Gerlai R (2020) Evolutionary conservation, translational relevance and cognitive function: The future of

727 zebrafish in behavioral neuroscience. Neurosci Biobehav Rev 116:426–435.

728 Glick SD, Sell EM, McCallum SE, Maisonneuve IM (2011) Brain regions mediating α3β4 nicotinic
729 antagonist effects of 18-MC on nicotine self-administration. Eur J Pharmacol 669:71–75.

730 Goodman WM, Spruill SE, Komaroff E (2019) A proposed hybrid effect size plus *p*-value criterion:
731 Empirical evidence supporting its use. Am Stat 73:168–185.

732 Gotti C, Zoli M, Clementi F (2006) Brain nicotinic acetylcholine receptors: native subtypes and their
733 relevance. Trends Pharmacol Sci 27:482–491.

734 Grant SA, Millar K, Kenny GN (2000) Blood alcohol concentration and psychomotor effects. Br J Anaesth
735 85:401–406.

736 Grasing K (2016) A threshold model for opposing actions of acetylcholine on reward behavior: Molecular
737 mechanisms and implications for treatment of substance abuse disorders. Behav Brain Res
738 312:148–162.

739 Haller G, Kapoor M, Budde J, Xuei X, Edenberg H, Nurnberger J, Kramer J, Brooks A, Tischfield J, Almasy
740 L, Agrawal A, Bucholz K, Rice J, Saccone N, Bierut L, Goate A (2014) Rare missense variants in
741 CHRNB3 and CHRNA3 are associated with risk of alcohol and cocaine dependence. Hum Mol Genet
742 23:810–819.

743 Herman AM, Ortiz-Guzman J, Kochukov M, Herman I, Quast KB, Patel JM, Tepe B, Carlson JC, Ung K,
744 Selever J, Tong Q, Arenkiel BR (2016) A cholinergic basal forebrain feeding circuit modulates
745 appetite suppression. Nature 538:253–256.

746 Ho J, Tumkaya T, Aryal S, Choi H, Claridge-Chang A (2019) Moving beyond P values: data analysis with
747 estimation graphics. Nat Methods 16:565–566.

748 Howe AS et al. (2016) Candidate genes in panic disorder: meta-analyses of 23 common variants in major
749 anxiogenic pathways. Mol Psychiatry 21:665–679.

750 Hua Y, Habicher J, Carl M, Manuel R, Boije H (2025) Novel Transgenic Zebrafish Lines to Study the
751 CHRNA3-B4-A5 Gene Cluster. Developmental Neurobiology 85:e22956.

752 Hu R, Dai Y, Jia P, Zhao Z (2018) ANCO-GeneDB: annotations and comprehensive analysis of candidate
753 genes for alcohol, nicotine, cocaine and opioid dependence. Database 2018 Available at:
754 http://dx.doi.org/10.1093/database/bay121.

755 Hwang WY, Fu Y, Reyon D, Maeder ML, Tsai SQ, Sander JD, Peterson RT, Yeh J-RJ, Joung JK (2013)
756 Efficient genome editing in zebrafish using a CRISPR-Cas system. Nat Biotechnol 31:227–229.

757 Jones AW (2019) Alcohol, its absorption, distribution, metabolism, and excretion in the body and
758 pharmacokinetic calculations. WIREs Forensic Science 1:e1340.

759 Kamens HM, Flarend G, Horton WJ (2023) The role of nicotinic receptors in alcohol consumption.
760 Pharmacol Res 190:106705.

761 Kamens HM, McKinnon CS, Li N, Helms ML, Belknap JK, Phillips TJ (2009) The alpha 3 subunit gene of the
762 nicotinic acetylcholine receptor is a candidate gene for ethanol stimulation. Genes Brain Behav
763 8:600–609.

764 Kibat C (2020) Functional Characterization of Nicotinic Acetylcholine Receptor Subunit ALPHA 3 in
765 Regulation of Behaviour.

766 Kily LJM, Cowe YCM, Hussain O, Patel S, McElwaine S, Cotter FE, Brennan CH (2008) Gene expression
767 changes in a zebrafish model of drug dependency suggest conservation of neuro-adaptation
768 pathways. J Exp Biol 211:1623–1634.

769 Koob GF, Vendruscolo L (2023) Theoretical Frameworks and Mechanistic Aspects of Alcohol Addiction:
770 Alcohol Addiction as a Reward Deficit/Stress Surfeit Disorder. Curr Top Behav Neurosci Available at:
771 http://dx.doi.org/10.1007/7854_2023_424.

772 Koskinen M-K, Hovatta I (2023) Genetic insights into the neurobiology of anxiety. Trends Neurosci
773 46:318–331.

774 Krishnan S, Mathuru AS, Kibat C, Rahman M, Lupton CE, Stewart J, Claridge-Chang A, Yen S-C, Jesuthasan
775 S (2014) The Right Dorsal Habenula Limits Attraction to an Odor in Zebrafish. Curr Biol 24:1167–
776 1175.

777 Kunst M, Laurell E, Mokayes N, Kramer A, Kubo F, Fernandes AM, Förster D, Dal Maschio M, Baier H
778 (2019) A Cellular-Resolution Atlas of the Larval Zebrafish Brain. Neuron 103:21–38.e5.

779 Kurta A, Palestis BG (2010) Effects of Ethanol on the Shoaling Behavior of Zebrafish (Danio Rerio). Dose
780 Response Available at: https://journals.sagepub.com/doi/10.2203/dose-response.10-008.Palestis
781 [Accessed October 17, 2023].

782 Lockwood B, Bjerke S, Kobayashi K, Guo S (2004) Acute effects of alcohol on larval zebrafish: a genetic
783 system for large-scale screening. Pharmacol Biochem Behav 77:647–654.

784 Maes HH, Neale MC, Chen X, Chen J, Prescott CA, Kendler KS (2011) A twin association study of nicotine
785 dependence with markers in the CHRNA3 and CHRNA5 genes. Behav Genet 41:680–690.

786 Manuel R, Iglesias Gonzalez AB, Habicher J, Koning HK, Boije H (2021) Characterization of Individual
787 Projections Reveal That Neuromasts of the Zebrafish Lateral Line are Innervated by Multiple
788 Inhibitory Efferent Cells. Front Neuroanat 15:666109.

789 Marks MJ, Pauly JR, Gross SD, Deneris ES, Hermans-Borgmeyer I, Heinemann SF, Collins AC (1992)

790 Nicotine binding and nicotinic receptor subunit RNA after chronic nicotine treatment. J Neurosci
791 12:2765–2784.

792 Mathur P, Berberoglu MA, Guo S (2011) Preference for ethanol in zebrafish following a single exposure.
793 Behav Brain Res 217:128–133.

794 Mathuru AS (2018) A little rein on addiction. Semin Cell Dev Biol 78:120–129.

795 Miller CN, Ruggery C, Kamens HM (2019) The α3β4 nicotinic acetylcholine receptor antagonist 18-
796 Methoxycoronaridine decreases binge-like ethanol consumption in adult C57BL/6J mice. Alcohol
797 79:1–6.

798 Miller N, Gerlai R (2007) Quantification of shoaling behaviour in zebrafish (Danio rerio). Behav Brain Res
799 184:157–166.

800 Miller N, Greene K, Dydinski A, Gerlai R (2013) Effects of nicotine and alcohol on zebrafish (Danio rerio)
801 shoaling. Behav Brain Res 240:192–196.

802 Moeller G, Terplan M (2020) Substance Use Disorders. Oxford University Press, USA.

803 Möykkynen T, Korpi ER (2012) Acute effects of ethanol on glutamate receptors. Basic Clin Pharmacol
804 Toxicol 111:4–13.

805 Nathan FM, Kibat C, Goel T, Stewart J, Claridge-Chang A, Mathuru AS (2022) Contingent stimulus
806 delivery assay for zebrafish reveals a role for CCSER1 in alcohol preference. Addict Biol 27:e13126.

807 Odstrcil I, Petkova MD, Haesemeyer M, Boulanger-Weill J, Nikitchenko M, Gagnon JA, Oteiza P, Schalek
808 R, Peleg A, Portugues R, Lichtman JW, Engert F (2022) Functional and ultrastructural analysis of
809 reafferent mechanosensation in larval zebrafish. Curr Biol 32:176–189.e5.

810 Ortiz-Guzman J, Swanson JL, Tantry EK, Kochukov M, Ung K, Addison AP, Srivastava S, Belfort BD, Ji E,
811 Dooling SW, Chen SA, Tong Q, Arenkiel BR (2024) Cholinergic Basal Forebrain Connectivity to the
812 Basolateral Amygdala Modulates Food Intake. eNeuro 11 Available at:
813 http://dx.doi.org/10.1523/ENEURO.0369-23.2024.

814 Oscar-Berman M, Marinković K (2007) Alcohol: Effects on Neurobehavioral Functions and the Brain.
815 Neuropsychol Rev 17:239–257.

816 Pichler P, Lagnado L (2020) Motor Behavior Selectively Inhibits Hair Cells Activated by Forward Motion in
817 the Lateral Line of Zebrafish. Curr Biol 30:150–157.e3.

818 Raj B, Farrell JA, Liu J, El Kholtei J, Carte AN, Navajas Acedo J, Du LY, McKenna A, Relić Đ, Leslie JM, Schier
819 AF (2020) Emergence of Neuronal Diversity during Vertebrate Brain Development. Neuron
820 108:1058–1074.e6.

821 Rehm J, Shield KD (2019a) Global Burden of Disease and the Impact of Mental and Addictive Disorders.
822 Curr Psychiatry Rep 21:10.

823 Rehm J, Shield KD (2019b) Global Burden of Alcohol Use Disorders and Alcohol Liver Disease.
824 Biomedicines 7:99.

825 Rima M, Lattouf Y, Abi Younes M, Bullier E, Legendre P, Mangin J-M, Hong E (2020) Dynamic regulation
826 of the cholinergic system in the spinal central nervous system. Sci Rep 10:15338.

827 Rueger SY, King AC (2013) Validation of the brief Biphasic Alcohol Effects Scale (B-BAES). Alcohol Clin Exp
828 Res 37:470–476.

829 Schmidt R, Strähle U, Scholpp S (2013) Neurogenesis in zebrafish - from embryo to adult. Neural Dev 8:3.

830 Schneider H, Pearson A, Harris D, Krause S, Tucker A, Gardner K, Chinyanya K (2023) Identification of
831 nicotine-seeking and avoiding larval zebrafish using a new three-choice behavioral assay. Front Mol
832 Neurosci 16:1112927.

833 Singleman C, Holtzman NG (2014) Growth and maturation in the zebrafish, Danio rerio: a staging tool for
834 teaching and research. Zebrafish 11:396–406.

835 Smith MA (2020) Nonhuman animal models of substance use disorders: Translational value and utility to
836 basic science. Drug Alcohol Depend 206:107733.

837 Sterling ME, Karatayev O, Chang G-Q, Algava DB, Leibowitz SF (2015) Model of voluntary ethanol intake
838 in zebrafish: effect on behavior and hypothalamic orexigenic peptides. Behav Brain Res 278:29–39.

839 Thorgeirsson TE et al. (2008) A variant associated with nicotine dependence, lung cancer and peripheral
840 arterial disease. Nature 452:638–642.

841 Tran S, Gerlai R (2013) Time-course of behavioural changes induced by ethanol in zebrafish (Danio rerio).
842 Behav Brain Res 252:204–213.

843 Tsang B, Ansari R, Gerlai R (2019) Dose dependent behavioral effects of acute alcohol administration in
844 zebrafish fry. Pharmacol Biochem Behav 179:124–133.

845 Varga TV, Hallmans G, Hu FB, Renström F, Franks PW (2013) Smoking status, snus use, and variation at
846 the CHRNA5-CHRNA3-CHRNB4 locus in relation to obesity: the GLACIER study. Am J Epidemiol
847 178:31–37.

848 Wada E, Wada K, Boulter J, Deneris E, Heinemann S, Patrick J, Swanson LW (1989) Distribution of alpha
849 2, alpha 3, alpha 4, and beta 2 neuronal nicotinic receptor subunit mRNAs in the central nervous
850 system: a hybridization histochemical study in the rat. J Comp Neurol 284:314–335.

851 Wen L, Jiang K, Yuan W, Cui W, Li MD (2016) Contribution of Variants in CHRNA5/A3/B4 Gene Cluster on
852 Chromosome 15 to Tobacco Smoking: From Genetic Association to Mechanism. Mol Neurobiol
853 53:472–484.

854 Witkiewitz K, Litten RZ, Leggio L (2019) Advances in the science and treatment of alcohol use disorder.
855 Sci Adv 5:eaax4043.

856 Xu W, Gelber S, Orr-Urtreger A, Armstrong D, Lewis RA, Ou CN, Patrick J, Role L, De Biasi M, Beaudet AL
857 (1999) Megacystis, mydriasis, and ion channel defect in mice lacking the alpha3 neuronal nicotinic
858 acetylcholine receptor. Proc Natl Acad Sci U S A 96:5746–5751.

859 Xu X, Scott MM, Deneris ES (2006) Shared long-range regulatory elements coordinate expression of a
860 gene cluster encoding nicotinic receptor heteromeric subtypes. Mol Cell Biol 26:5636–5649.

861 Yang W, Singla R, Maheshwari O, Fontaine CJ, Gil-Mohapel J (2022) Alcohol Use Disorder: Neurobiology
862 and Therapeutics. Biomedicines 10:1192.

863 Zhou X, Zheng W, Li Y, Pearce R, Zhang C, Bell EW, Zhang G, Zhang Y (2022) I-TASSER-MTD: a deep-
864 learning-based platform for multi-domain protein structure and function prediction. Nat Protoc
865 17:2326–2353.

866

867 ## Figure & Table Legends

868 **Table 1.** Primers for single-guide RNA template. CRISPR targets are underlined. Homology arms in lower
869 case.

870

871 **Table 2.** Mean time spent by zebrafish in the stimulus chamber during SAZA over an 18 minute stimulus
872 dispensing period (n = 30-32)
873
874 **Table 3.** Primers used for qPCR of *chrna3*, *chrna5*, *chrnb4*, and housekeeping genes.
875
876 **Table 4.** Probe sequences for FISH-HCR. B1 Probes were visualised with Alexa fluorophore 546, B2
877 probes were visualised with Alexa fluorophore 647, and B3 probes were visualised with Alexa
878 fluorophore 488. P1 and P2 probes of the same gene are paired according to number 1-8.
879
880 **Table 5.** Genes included in the custom sets 'Nicotine dependence ' and 'Alcohol dependence'. These
881 genes have been associated with nicotine and alcohol dependence, described by Hu *et al.* (Hu et al.
882 2018)
883
884 **Figure 1**. **Self-Administration Zebrafish Assay (SAZA) chamber functional design and characterisation**
885 **of the *chrna3*$^{C246X}$ mutant zebrafish.**
886 **A.** Schematic indicating locations of inflow of system water (In, top) and outflow (Out, centre). Control
887 and stimulus delivery inlets (stimulus shown in purple) are activated when a fish enters the
888 corresponding zone. Continuous inflow and outflow constrain the stimulus/control delivered to their
889 respective zones (Nathan et al., 2022) . 'Measurement area' denotes where alcohol concentration was
890 measured in panel C. **B.** Schematic shows the experimental design with three minute pre- and post-
891 exposure periods before and after an 18 minute self-administration period. Representative sparklines
892 plots show the entries and duration (thickness) of entry of the subject fish either into the stimulus or the
893 control zones when 20% or 70% alcohol is used as stimuli. **C.** Alcohol concentrations measured when

894 20% or 70% alcohol were dispensed for the duration mimicking subject fish behaviour (± standard
895 error). The average concentration (solid line) fish experience is 0.5% and 1.5% alcohol respectively. See
896 Table 2 for additional details. **D-H.** Characterisation of *chrna3*$^{C246X}$ mutant fish**. D**. *chrna3*$^{C246X}$ mutants
897 have a premature stop codon in the transmembrane region 1, amino acid 246 (M1 - red star), due to the
898 indel of 5bp at position 786bp. **E.** Predicted protein structure of chrna3 in WT and *chrna3*$^{C246X}$ mutants,
899 generated by iTasser (Zhou et al., 2022), colour coded by domain. **F.** Fold change of *chrna3* in 12 week
900 old WT (n = 21) vs. *chrna3*$^{C246X}$ (n = 20) by qRT-PCR. **G-H.** *chrna3* expression in 14 day old zebrafish larvae
901 visualised by Hybridisation Chain Reaction™ RNA-FISH (HCR™) in the **G.** Predicted facial motor nucleus
902 (Fmn) marked by *chata* expression and, **H.** dorsal habenula (dHb) marked by *nrp1a* expression, in WT
903 and *chrna3*$^{C246X}$ respectively. Images are representative, see figures S1 and S2 for replicates
904 (WT/*chrna3*$^{C246X}$ Fmn n = 3/4, dHb n = 4/3). Schematic images with regional markers (v2.0, MECE, 2024)
905 were generated in mapZeBrain Atlas (mapzebrain.org, May 2025) (Kunst et al., 2019). Hb = habenula,
906 vHb = ventral habenula, Omn = oculomotor nucleus, Trm = trochlear motor nucleus, Ni = nucleus isthmi,
907 Vmn = vagus motor nucleus, srFmn = supra-rostral Fmn, rFmn = rostral Fmn, cFmn = caudal Fmn. Genes
908 presented left to right: all genes merged, **G.** *chata* or **H.** *nrp1a*, *chrna3*, *elavl3*, and *chrna3* with false
909 colour post-processing. False colour adjusted (fc) and elavl3 images have been brightened for enhanced
910 visibility.

911

912 **Figure 2. The preference for alcohol is biphasic.**

913 Gardener-Altman and Cumming estimation plots show alcohol response in three-minute intervals. No
914 stimulus was dispensed in the 'Pre' and 'Post' periods. Time spent in the stimulus zone during x̄0.5%
915 SAZA condition for **A.** WT (n = 31) and **D.** *chrna3*$^{C246X}$ mutants (n = 32). Time spent in the stimulus zone in
916 the x̄1.5% SAZA condition for **B.** WT (n = 30) and for **E.** *chrna3*$^{C246X}$ mutants (n = 30). **C.** Ethanol
917 concentrations in the stimulus zone in the x̄0.5% and x̄1.5% alcohol conditions and estimated for

extended periods. The concentration at which attraction switches to aversion is highlighted. Asterisks indicate a significant paired mean difference between that time portion and the pre-stimulus period: * = $p_{adj} < 0.05$ (provisional difference), ** = $p_{adj} < 0.01$ (meaningful difference). See Table S1 for the precise effect sizes and p-values, corrected for multiple comparisons.

**Figure 3. *chrna3* mutation dynamically alters relative preference for alcohol.**

**A-C.** Gardener-Altman and Cumming estimation plots comparing the volume of alcohol dispensed over the entire self-administration period during SAZA for **A.** WT (0%/x̄0.5%/x̄1.5%, n = 30/31/30), **B.** *chrna3*$^{C246X}$ (0%/x̄0.5%/x̄1.5%, n = 29/32/30) and **C.** intergenotype comparisons. Asterisks indicate the following significant differences from 0% alcohol treatments (**A, B**), or the WT (**C**): * = $p_{adj} < 0.05$, and effect size reported by Cliff's delta between ± 0.2 and ± 0.4 (provisional difference), ** = $p_{adj} < 0.01$ and effect size bigger than ± 0.4 (meaningful difference). **D-I**. Paired mean difference of preference index (PI) between **D-F.** Pre and 0-9m or **G-I.** 0-9 and 9-18m time periods within genotypes, and delta delta comparisons between genotypes, during **D, G.** 0%, **E, H.** x̄0.5%, and **F, I.** x̄1.5% SAZA. Asterisks indicate a significant paired mean difference, or delta delta, between time periods: * = $p < 0.05$ (provisional difference), ** = $p < 0.01$ (meaningful difference). See Table S2 for the exact effect size and p-values.

**Figure 4. *chrna3* mutants experience reduced psychoactive effects from alcohol exposure. A.** Schematic outline of the shoaling assay metric calculation and processing steps for cohesion (shoal area) and kinesis (shoal movement). **B, C.** Gardener-Altman, or **D, F, H.** mean (± 95% CI) shoal cohesion, and **E, G, I.** kinesis, with Cumming estimation plots for the shoaling cohesion assay showing **B, D, E.** WT, **C, F, G.** *chrna3*$^{C246X}$, and **H, I.** intergenotype comparisons. Metrics recorded per frame at 2fps (n = 6 assays per genotype, per treatment). Asterisks indicate a significant difference in the estimated marginal mean from **B-G.** 0% alcohol, or **H, I.** WT within that time period: * = $p_{adj} < 0.05$, and effect size reported by

942 Cliff's delta between ± 0.2 and ± 0.4 (provisional difference), ** = $p_{adj}$ < 0.01 and effect size greater than
943 ± 0.4 (meaningful difference). See Table S3 for exact effect size and p-values.
944
945 **Figure 5. *chrna3*$^{C246X}$ mutants exhibit transcriptional changes in dependence, neuronal development,**
946 **and ion channel process associated genes.** RNAseq comparison of *chrna3*$^{C246X}$ (n = 3) vs *chrna3*$^{C246X}$ (n =
947 3) 12 week old zebrafish whole brain tissues. **A.** PCA clustering of samples by genotype. **B.** All
948 significantly enriched GO terms between genotypes. Positive enrichment values indicate enrichment in
949 the *chrna3*$^{C246X}$ mutant zebrafish. Significance thresholds are defined at *p* = < 0.05 and FDR < 0.2. Yellow
950 = secondary messenger associated, Blue = ion channel associated, pink = neuronal differentiation and
951 development, green = behaviours. **C.** Volcano plot of gene expression changes between genotypes.
952 Up/down-regulated genes = *p* < 0.05 & log2 fold change > ±2. Provisional up/down-regulated genes = *p* <
953 0.05 & log2 fold change < ±2. Not significant genes = *p* > 0.05. The colour key applies to D-F and I-K.
954 Positive fold change values indicate up-regulation in the *chrna3*$^{C246X}$ mutant zebrafish. **D-F.** Subsets of
955 volcano plot **C**, highlighting **D.** glutamate, **E.** GABA, and **F.** nicotinic acetylcholine (nAChR) receptor gene
956 families. **G.** Mean counts (± standard deviation) of nAChRs (gene prefix 'chrn'). Stars indicate significant
957 difference between genotypes, ** = p < 0.01, * = p < 0.05. **H.** Fold change in WT vs *chrna3*$^{C246X}$ of *chrna5*
958 (n = 21/20) and *chrnb4* (n = 22/22) by qRT-PCR. Stars indicate significant difference between genotypes,
959 ** = p < 0.01, * = p < 0.05. **I-K.** Subsets of volcano plot **C**, highlighting genes associated with **I.** nicotine or
960 **J.** alcohol dependence (Hu et al., 2018), and **K.** anxiety phenotypes (Howe et al., 2016; Koskinen and
961 Hovatta, 2023). The full gene lists can be found in Table 4.
962

963 ## Movie Legends

964

965 **Movie 1:** A representative segment of the zebrafish self-administration assay (SAZA) with x̄1.5% alcohol
966 shown in Figure 1B.
967
968 **Movie 2:** A representative segment of the shoaling assay with 1% alcohol shown in figure 4D.
969

## 970 Supplementary Figure & Table Legends

971
972 **Figure S1.** Replicates of *chrna3* expression from figure 1, in *WT* (**A**) and *chrna3*$^{C246X}$ (**B**) 14dpf zebrafish
973 larvae facial motor nucleus (Fmn) marked by *chata* expression, visualised by *in-situ* hybridisation chain
974 reaction (HCR). Scale bars = 10 µm. **C.** Comparison of the mean fluorescent intensity (± standard
975 deviation) of *chrna3* in the demarcated zone between genotypes (Mean difference = -24.0 [95CI -26.3,-
976 20.9], p = 0.012).
977
978 **Figure S2.** Replicates of *chrna3* expression from figure 1, in *WT* (**A**) and *chrna3*$^{C246X}$ (**B**) 14dpf zebrafish
979 larvae right dorsal habenula (Hb) marked by *nrp1a* expression, visualised by *in-situ* hybridisation chain
980 reaction (HCR). Scale bars = 20 µm. **C.** Comparison of the mean fluorescent intensity (± standard
981 deviation) of *chrna3* in the demarcated zone between genotypes (Mean difference = 0.168 [95CI -2.84,
982 1.73], p = 0.944).
983
984 **Figure S3.** Gardener-Altman and Cumming estimation plots show alcohol response in three-minute
985 intervals. No stimulus was dispensed in the 'Pre' and 'Post' periods. Time spent in the stimulus zone
986 during 0% SAZA condition for **A.** WT (n = 31) and **B.** *chrna3*$^{C246X}$ mutants (n = 32). Time spent in the
987 control zone for **C, E, G.** WT (n = 30/31 /30) and **D, F, H.** *chrna3*$^{C246X}$ mutants (n = 29/32/30) in **C, D.** 0%,
988 **E, F.** x̄0.5% and **G, H.** x̄1.5% SAZA. Asterisks indicate a significant difference between that time portion

989 and the pre-stimulus period: * = $p_{adj} < 0.05$ ** = $p_{adj} < 0.01$. See Table S1 for the precise effect sizes and

990 p-values, corrected for multiple comparisons.

991

992 **Figure S4.** Gardener-Altman and Cumming estimation plots show alcohol response in three-minute

993 intervals. No stimulus was dispensed in the 'Pre' and 'Post' periods. Number of entries into the stimulus

994 zone for **A-C.** WT (n = 30/31 /30) and **D-F.** *chrna3*$^{C246X}$ mutants (n = 29/32/30) in **A, D.** 0%, **B, E.** x̄0.5% and

995 **C, F.** x̄1.5% SAZA. Asterisks indicate a significant difference between that time portion and the pre-

996 stimulus period: * = $p_{adj} < 0.05$ ** = $p_{adj} < 0.01$. See Table S1 for the precise effect sizes and p-values,

997 corrected for multiple comparisons.

998

999 **Table S1**. Statistical analysis output table for Figure 2 A-E, and Figures S3 and S4, intragenotype paired

1000 mean difference of % time in stimulus, time in control, or number of entries, for repeated measures

1001 against the 'Pre' period for 0%, x̄0.5% and x̄1.5% alcohol SAZA.

1002

1003 **Figure S5.** Gardener-Altman and Cumming estimation plots for total SAZA self-administration period for

1004 WT (**A, D**), *chrna3*$^{C246X}$ (**B, E**) and comparisons (**C, F**). Plots display the comparison of velocity inside (**A- C**)

1005 or outside (**D-F**) the stimulus zone at different concentrations (0/x̄0.5/x̄1.5%) for WT (n = 30/31/30) and

1006 *chrna3*$^{C246X}$ zebrafish (n = 29/32/30). **G-I.** Gardener-Altman and Cumming estimation plots for **G.** 0%, **H.**

1007 x̄0.5%, and **I.** x̄1.5% SAZA. Plots compare preference index (PI) between WT (0/x̄0.5/x̄1.5% n = 30/ 31/30)

1008 and *chrna3*$^{C246X}$ (0/x̄0.5/x̄1.5% n = 29/32/30) within each time period. No stimulus was dispensed in the

1009 'Pre' and 'Post' periods. Asterisks indicate the following significant differences from 0% alcohol

1010 treatments (**A, B, D, E**) or WT (**C, F-I**): * = $p < 0.05$, and effect size reported by Cliff's delta between ± 0.2

1011 and ± 0.4 are considered provisional, ** = $p < 0.01$ and effect size bigger than ± 0.4 is considered a

1012 meaningful difference. See Table S2 for exact effect size and p-values.

1013

1014 **Figure S6**. Cliff's delta (± 95% CI) forest plots of all calculated metrics from 0/x̄0.5/x̄1.5% alcohol SAZA,

1015 comparing the response of wild type to *chrna3*$^{C246X}$ mutant zebrafish. Positive values indicate a greater

1016 response in the mutant. See Table S2 for exact effect size and p-values.

1017

1018 **Table S2.** Statistical analysis output table for figure 3A, B, intragenotype, and figure 3C, intergenotype,

1019 comparisons of stimulus volume dispensed over the full self administration period for 0, x̄0.5 and x̄1.5%

1020 alcohol SAZA. Statistical analysis output table for figure 3 D-I, paired mean difference and delta-delta in

1021 preference index (PI) between time periods, Figure S5 A-C, comparing preference index (PI), velocity,

1022 and Figure S6 other metrics for 0, x̄0.5 and x̄1.5% alcohol SAZA.

1023

1024 **Figure S7**. ***WT* and *chrna3*$^{C246X}$ mutants share shoaling cohesion and kinesis phenotypes during 0% and**

1025 **1% alcohol immersion.** Mean (± 95% CI) shoal cohesion (**A, C**) and kinesis (**B, D**) with Cumming

1026 estimation plots comparing 0% (**A, B**), or 1% alcohol exposure (**C, D**) between genotypes. Metrics

1027 compared per frame at 2fps (n = 6 assays per genotype, per treatment). Asterisks indicate the following

1028 significant differences from WT within that time period: * = $p < 0.05$, and effect size reported by Cliff's

1029 delta between ± 0.2 and ± 0.4 are considered provisional, ** = $p < 0.01$ and effect size bigger than ± 0.4

1030 is considered a meaningful difference. See Table S3 for exact effect size and p-values.

1031

1032 **Table S3.** Statistical analysis output table for figure 4A-G, comparing shoaling behaviours within

1033 genotype, figure 4H-I and S7, between genotypes, displaying pairwise effect size comparisons, and

1034 repeated measures estimated marginal mean difference adjusted p values within time period.

**Figure 1** Raine, Kibat, *et. al* 2025

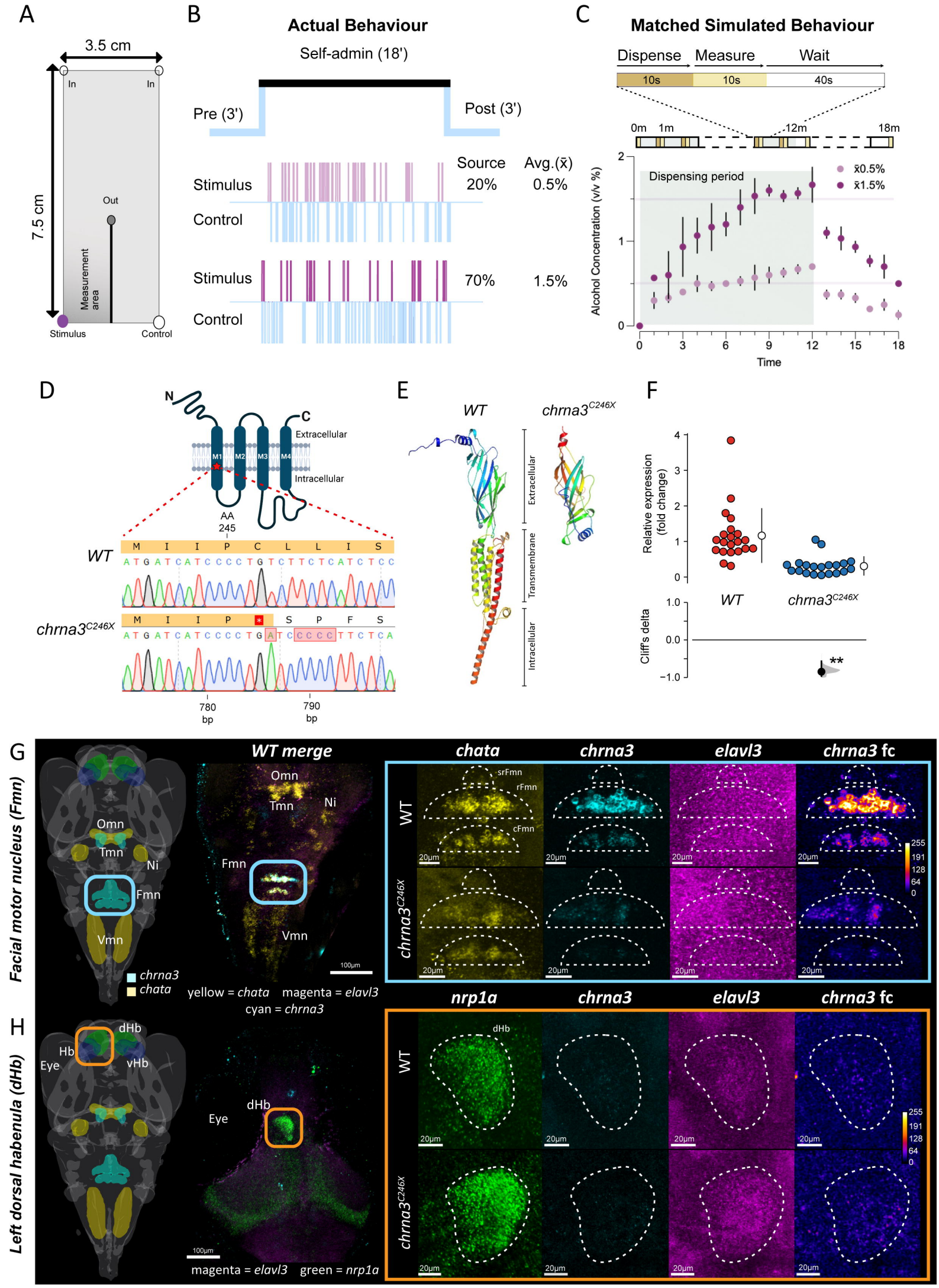

**Figure 5**

Raine, Kibat, *et. al* 2025

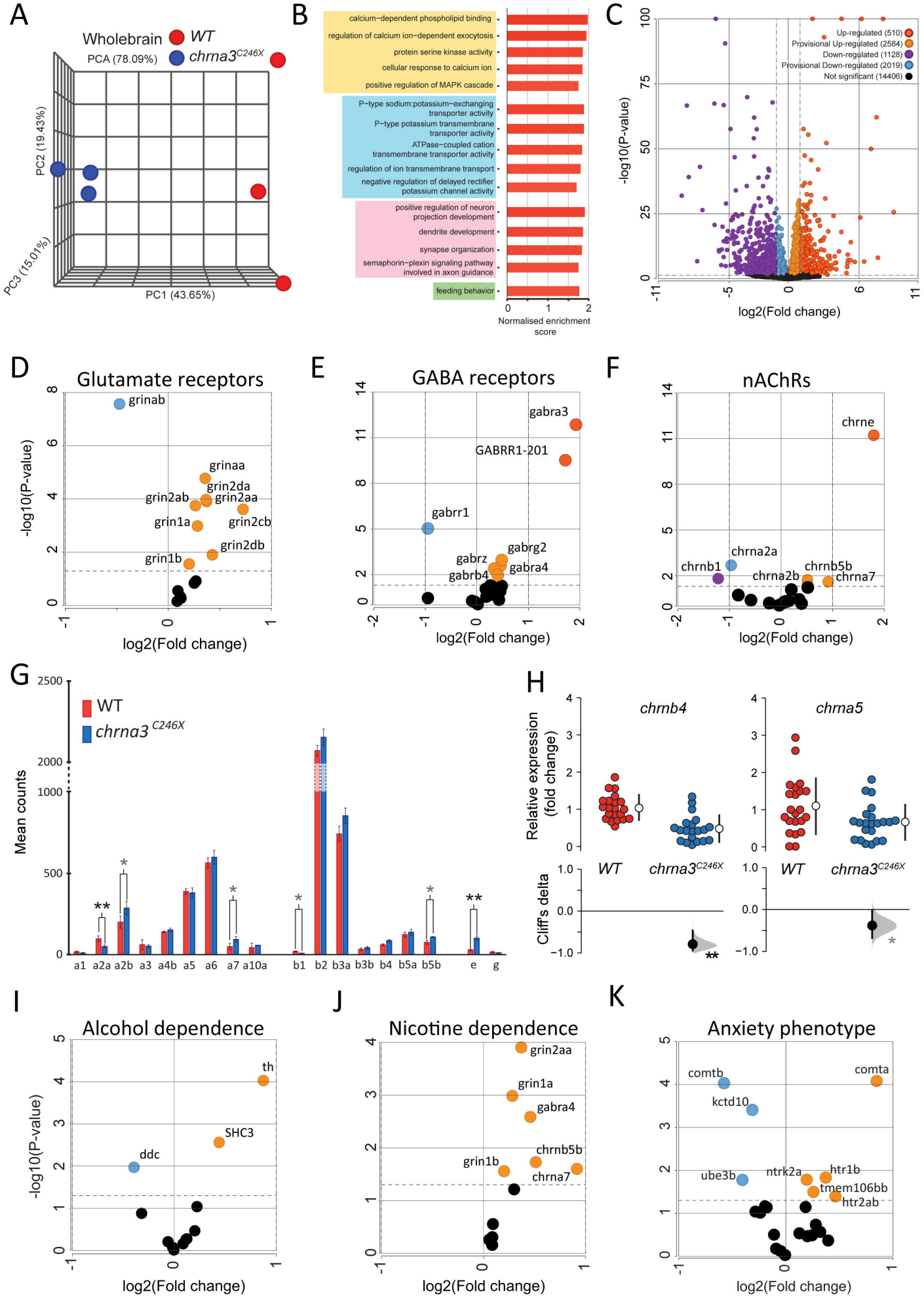

**Figure 4**

Raine, Kibat, *et. al* 2025

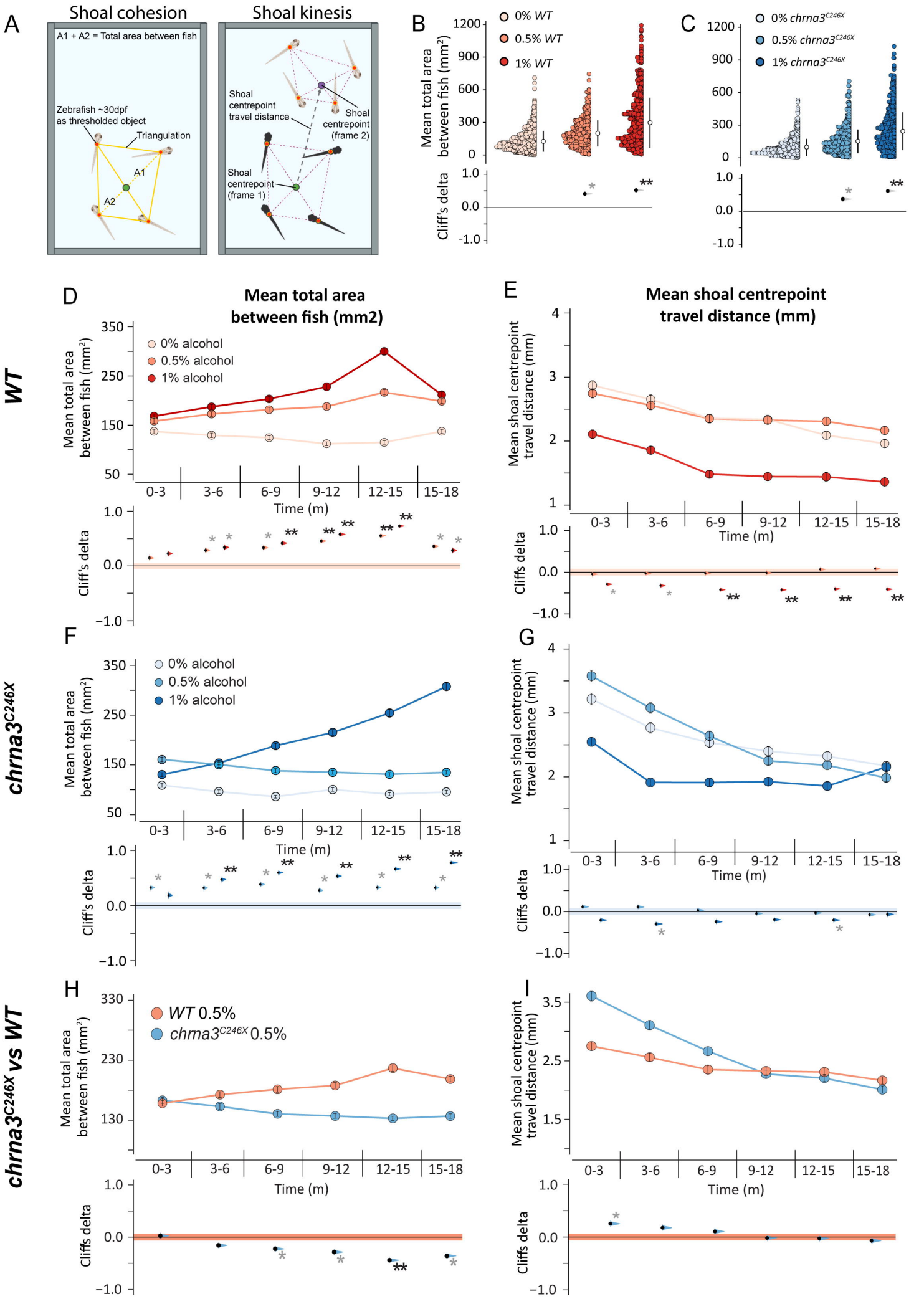

**Figure 3**

Raine, Kibat, *et. al* 2025

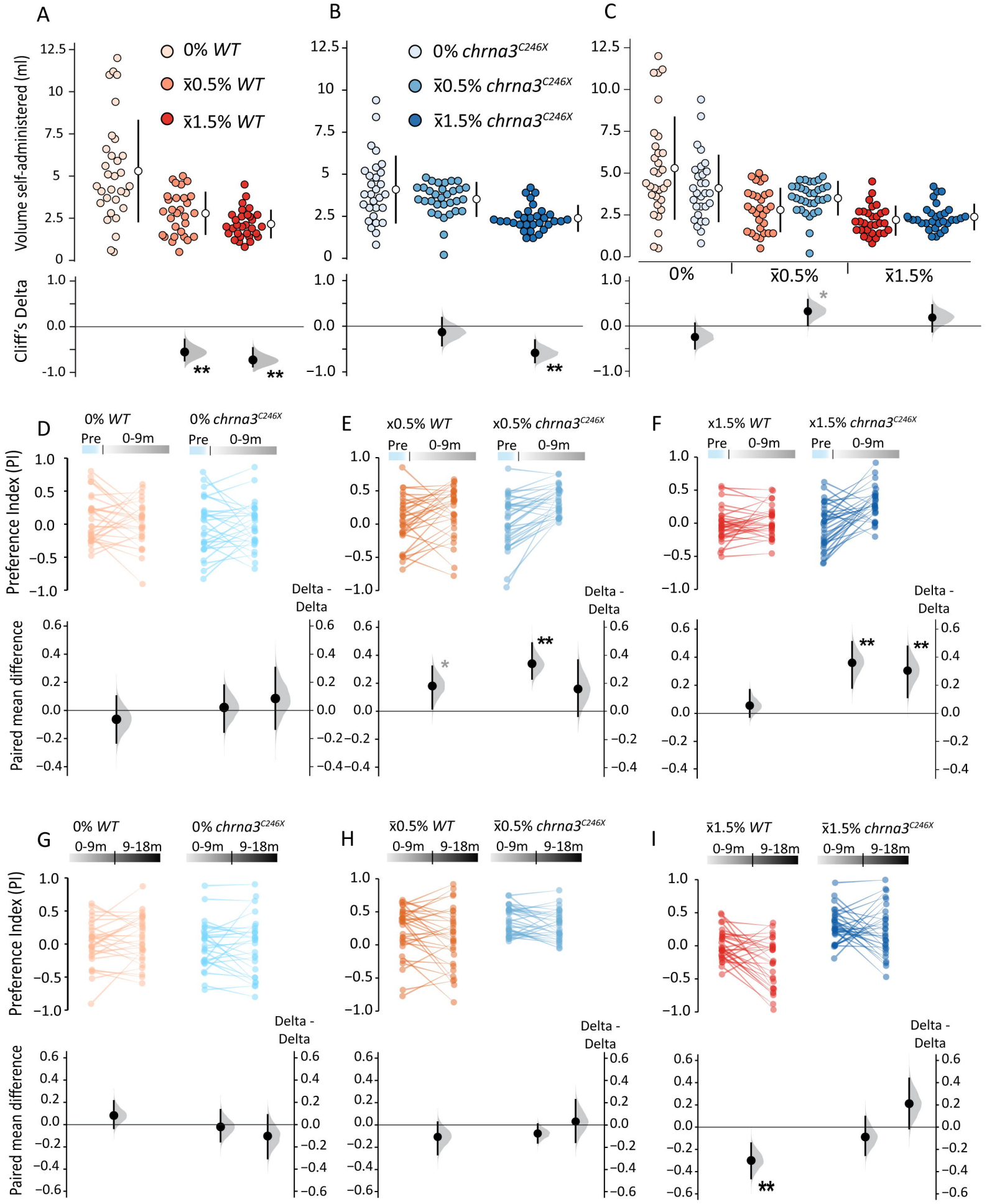

**Figure 2**
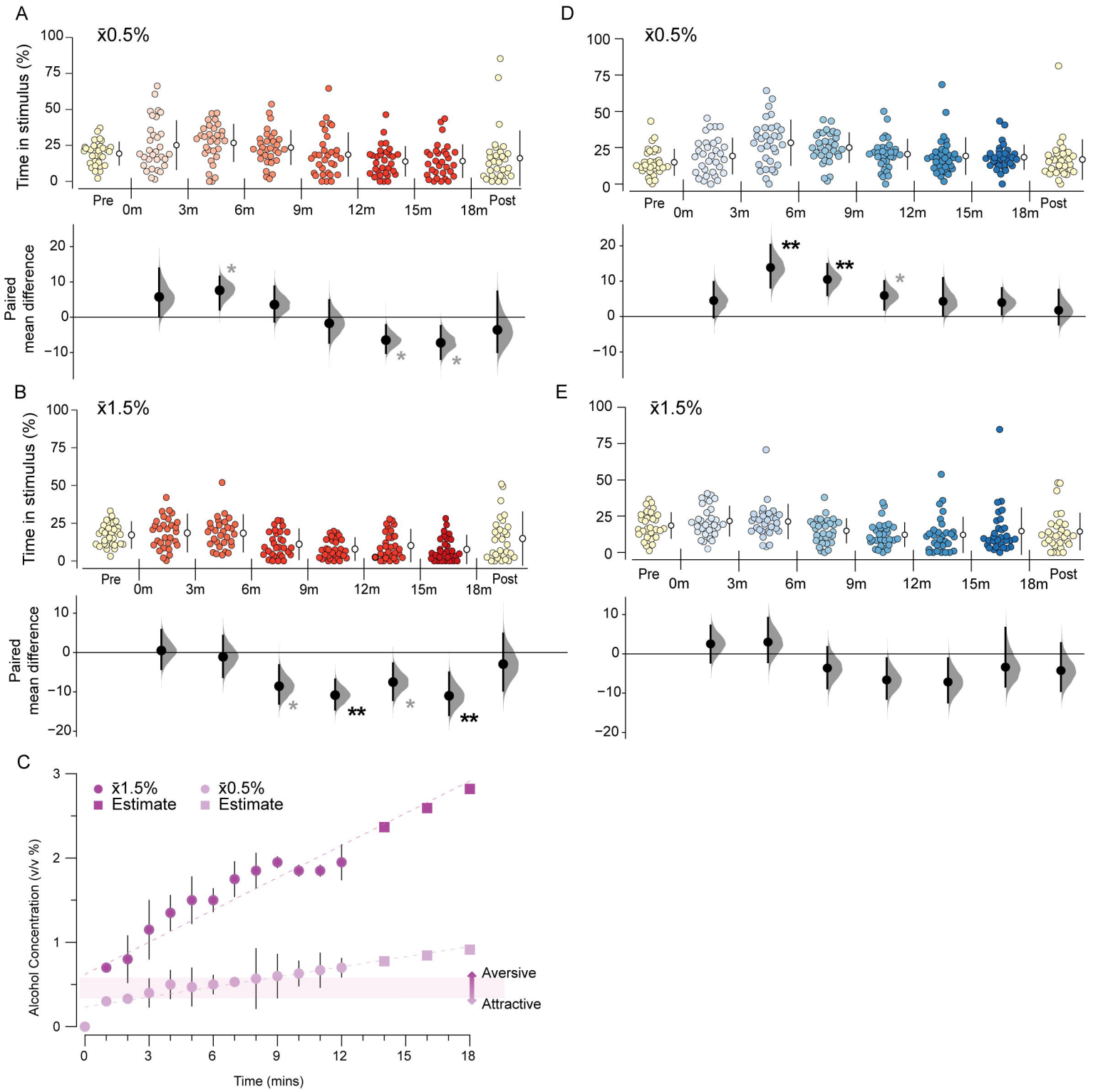
Raine, Kibat, *et. al* 2025